12-2020

3D Printed Microporous Collagen Constructs Using the Freeze-FRESH Methodology

Thais Sousa Senzano

3D Printed Microporous Collagen Constructs Using the Freeze-FRESH Methodology

by

Thais Sousa Senzano

A thesis submitted to the College of Engineering and Science of
Florida Institute of Technology
in partial fulfillment of the requirements
for the degree of

Master of Science
In
Biomedical Engineering

Melbourne, Florida
December 2020

We, the undersigned committee, hereby approve the attached thesis, “3D Printed Microporous Collagen Constructs Using the Freeze-FRESH Methodology” by Thais Sousa Senzano, be accepted as fulfilling in part the requirements for the degree of Master of Science in Biomedical Engineering

Vipuil Kishore, Ph.D.
Associate Professor
Biomedical and Chemical Engineering and Sciences
Thesis Advisor

Linxia Gu, Ph.D.
Professor
Biomedical and Chemical Engineering and Sciences
Committee Member

Julia Grimwade, Ph.D.
Professor
Biomedical and Chemical Engineering and Sciences
Committee Member

D. Andrew Knight, Ph.D.
Professor and Department Head
Biomedical and Chemical Engineering and Sciences

Abstract

3D Printed Microporous Collagen Constructs Using the Freeze-FRESH Methodology

Author: Thais Sousa Senzano

Advisor: Vipuil Kishore, Ph.D.

Scaffold microporosity is known to play a critical role in governing cellular response including cell migration, proliferation, and tissue-specific differentiation. While fabrication approaches such as solvent leaching and freeze-casting are commonly used for the generation of microporous biomaterial scaffolds, these methods provide little control over scaffold geometry and creation of complex tissue structures. Extrusion-based 3D printing, an additive manufacturing method, is a highly versatile layer-by-layer printing approach that allows for the fabrication of easily customizable 3D scaffolds with complex architecture using a vast selection of polymeric bioinks. These 3D printed constructs are porous at the macroscale, but achieving microporosity (i.e., < 100 μm) in printed constructs is challenging due to the sub-optimal resolution of the extrusion-based printing method. A recent study using alginate inks introduced a new fabrication technique termed Freeze-FRESH (FF) that combines extrusion printing and freeze-casting approaches to generate 3D constructs with hierarchical microporosity. However, the porosity of the resultant alginate constructs was comparable despite changing the freezing temperature. In the

current study, the FF method was modified to print collagen constructs with greater control of microporous architecture. Highly concentrated collagen type I ink was used to 3D print collagen constructs using the freeform reversible embedding of suspended hydrogels (FRESH) approach. Modification of the FF technique entailed melting of the FRESH bath post printing via incubation at 37 °C followed by freezing and lyophilization to allow for collagen gelation and better heat transport during the freezing process. The effect of freezing temperature on micropore size, swelling degree, degradation, and mechanical properties of printed constructs was assessed. Finite element (FE) models were generated to predict the mechanical properties of microporous scaffolds. In addition, the effect of microporosity on Saos-2 cell morphology, proliferation, infiltration, and ALP activity was evaluated. Results from the study showed that freezing temperature effectively modulated micropore size and that constructs with larger micropore size were more stable. Microporosity had no effect on swelling ratio yet caused a decrease in mechanical properties of collagen constructs; FE models confirmed experimental results. Cell metabolic activity and infiltration was enhanced in microporous constructs with larger pore size, yet there was no effect on cell morphology, and ALP activity. In conclusion, the modified FF technique can be effectively used to fabricate hierarchically porous 3D collagen constructs.

Table of Contents

List of Figures

List of Tables

Acknowledgements

I would like to profoundly thank Dr. Vipuil Kishore for his guidance, continuous support, and for teaching me so many valuable lessons that I will carry forever throughout my life. I am deeply grateful to him for giving me the opportunity to look deeper, learn, challenge myself in unimaginable ways, and for helping me build strong skills as a researcher.

I would like to also thank Nilabh Kajave and Trevor Schmitt for always helping me when I needed the most and for sharing their knowledge and expertise with me in the lab. Thank you for making the lab an enjoyable workspace where we always had each other's back. I would also like to thank Dr. Linxia Gu and Dr. Pengfei Dong for bringing such a positive energy and for contributing to this work with the mechanical testing and FE modeling. Also, to Dr. Stephanie Florczyk, for giving us valuable insight and for contributing to this project. I would also like to thank Gayle Duncombe for her help and support at the microscopy center as well as Tatiana Karpova for her words of encouragement during my long working hours.

To my friends, Andressa Camacho, Nicolas Irurita, Malu Leon, Ralston D'Cunha, Oriana Valladares, Julian Robledo: Thank you for being my main support system, for sharing with me so many unforgettable moments, and for being my family away from home. To Jicmat Ali Tribaldos, I cannot express how grateful I am

to have you in my life. Thank you for being there every step of the way, for keeping me motivated, for being my safe place, and for always believing in me!

Finally, and most importantly, I would like to thank my parents, my grandparents, and my siblings for their constant support, encouragement, and unconditional love. Thank you for sharing with me your words of wisdom, for constantly inspiring me to grow and achieve great things, and for showing me that anything is possible. Without you, I would not be where I am today!

Dedicated to my parents, grandparents, and my siblings

Chapter 1

Introduction

In a currently ever-expanding aging population, tissue and organ failure due to disease or injury has become a main socioeconomic and healthcare burden, accounting for about half of the total healthcare expenditure in the United States [1]. The present clinical strategy to address this problem is the use of donated tissues and utilize them as allografts or xenografts. However, donors are extremely limited and unable to meet the increasing demand for tissue and organ transplantations. In addition, there is a significant risk of patient immune rejection of transplants from foreign sources and the possibility of disease transmission. Autografts are expensive, anatomically limited, and related to donor-site morbidity [2]. Tissue engineering (TE) has garnered significant interest over the past few decades as a promising alternative solution to address this important clinical need. TE is a rapidly developing multidisciplinary field that adopts knowledge and strategies from areas such as biology, chemistry, materials science, genetics, medicine, and engineering to create products and therapies to repair or replace damaged tissues and organs [3].

Significant efforts have been made to develop biomaterial scaffolds to guide the repair of damaged tissues. A suitable biomaterial scaffold must be biocompatible, biodegradable, have appropriate mechanical properties, and adequate surface architecture [2]. Biomaterial scaffolds are usually seeded with cells and optionally

supplemented with growth factors and/or external stimuli, such as mechanical forces, to guide the synthesis of new tissue by cells. Most importantly, ideal scaffolds must be designed to house cells with appropriate biochemical, mechanical, and topographical cues to direct regenerative behavior. Furthermore, the scaffold architecture must possess a network of interconnected pores to allow cell penetration and support cell growth by enabling the transport of nutrients and wastes from and into the scaffold. Microporous scaffold architecture not only allows for the exchange nutrients and wastes but has also been shown to improve cell infiltration [4], direct cell behavior and differentiation [5–7]. Both synthetic and natural biomaterials have been extensively used, with natural polymers having superior biological properties such as the presence of cell adhesion protein sequences [8]. Among these, collagen type I is an ideal biomaterial due to its excellent biocompatibility, innate biodegradability, and low immunogenicity [9].

A multitude of fabrication methods are used to produce collagen scaffolds for tissue engineering applications. These include particulate leaching [10], freeze-casting [11], electrospinning [12], electrochemical alignment [13], and 3D printing [14]. In the recent past, extrusion-based 3D printing has garnered significant interest as a fabrication method due to ease of use, wide range of polymeric hydrogel-based inks to produce tissue constructs, and precision printing of complex structures [15]. Hydrogel-based inks are suitable for 3D printing due to their ability to flow, ease of extrusion given their shear-thinning properties, rapid solidification post-printing

using chemical or physical stimuli, and ability to load cells and/or bioactive molecules [16]. Collagen hydrogels provide a favorable environment to cells replicating the natural extracellular matrix (ECM) with high water content, porous structure, and adjustable mechanical and degradation properties. Nevertheless, collagen hydrogels have weak mechanical properties and are difficult to be used as an ink for 3D printing since the printed structures are unable to support their weight and maintain their shape post-printing. Freeform reversible embedding of hydrogels (FRESH) printing approach uses a biocompatible gelatin support bath to enable printing of soft hydrogel inks by providing structural support for layer-by-layer material deposition and generation of 3D constructs with improved print fidelity [17]. However, challenges associated with limited print resolution exist when attempting to incorporate microporous features of less than 100 microns into 3D printed constructs.

Recently, FRESH 3D printing was combined with freeze-casting to produce hierarchically porous alginate constructs with a technique termed the Freeze-FRESH (FF) method [18]. This method entails printing a 3D construct onto the gelatin support bath and immediately freeze-drying the constructs while embedded in the support medium. However, in the present study, the FF method was modified to yield porous collagen constructs with different micropore sizes. 3D printed constructs were incubated at 37 °C prior to the freeze-drying steps to allow the gelation of collagen constructs and melt the gelatin into a liquid medium. This critical step

ensured construct stability and better heat transfer of the convective medium for the subsequent freezing process. The hypotheses of this study include (i) changing the freezing temperature during the FF process will modulate the micropore size of 3D printed collagen constructs, (ii) micropore size will impact the physical and mechanical properties of 3D printed collagen constructs, (iii) larger micropore size will enhance cell infiltration and proliferation and, (iv) micropore size will modulate Saos-2 cell ALP activity.

The next chapter will outline a brief background on different fabrication and processing strategies to produce porous biomaterial scaffolds with a focus on 3D printing and the FF method. Chapter III details the fabrication and characterization of 3D printed collagen constructs using the modified FF methodology, as well as the results and discussion of the effect of microporosity on Saos-2 cell response. Conclusions from the study and potential future work are discussed in Chapter IV.

Chapter 2

Literature Review

2.1. Microporosity

One of the most important design aspects of biomaterial scaffolds is porosity. The presence of porosity is vital for improved cell attachment, cell seeding efficiency, migration towards the core of the scaffold, exchange of metabolites, tissue ingrowth, and development of vascularization. Porous scaffold architectures must be directed by components such as pore size, morphology, degree of interconnectivity, and overall porosity which play a significant role in biological delivery and tissue regeneration [19,20]. Cells interact with the scaffold surface primarily through chemical ligands or adhesion sites (i.e. Arg-Gly-Asp peptide sequence) [2]. Ligand density is affected by the specific surface area of the scaffold available for cells to attach. Thus, scaffold pore size must be sufficiently large to allow migration and infiltration of cells into the scaffold as well as maintain a high enough specific surface area to allow a critical number of cells to adhere [21]. A crucial range of pore size exists depending specifically on the cell type and tissue [22,23]. On the other hand, pore morphology not only allows cells to migrate but also affects the degree of cell proliferation and differentiation into various lineages [5,24,25]. The arrangement of pores and pore morphologies are able to control cell proliferation, modulate levels of cell differentiation markers, and direct cell fate [26]. Another important component to consider is overall scaffold porosity. A trade-off exists between

biological activity and mechanical properties. Increased porosity and pore size facilitate tissue ingrowth; however, the structural integrity of scaffolds is compromised and mechanical performance is decreased [27]. Hence, the choice of optimal scaffold characteristics essentially depends on the biological and mechanical needs of specific applications.

While porosity can be present at various length scales, a hierarchical organization of pores enables to closely replicate the complex architecture of native tissues such as skin and bone [28]. For long, researchers have been interested in producing biomimetic scaffolds with a hierarchically structured organization as well as a variety of pores ranging from nanometer to micrometer scales [29,30]. For example, scaffolds with compositional and architectural similarity to cancellous bone showed the most optimal environment for osteoblast attachment, proliferation, nutrient exchange, and deposition of collagen and mineral bone [29]. Thus, replicating the architectural complexity of tissues can significantly increase and optimize scaffold bioactivity.

2.2. Fabrication Methods of Porous Biomaterial Scaffolds

A myriad of fabrication methods exist to produce porous polymer-based scaffolds with a large variety of properties. These methods include freeze-drying,

particle leaching, gas foaming, and electrospinning [28]. Freeze-drying is the most common technique to create random porosity in polymeric scaffolds. This method entails freezing a liquid slurry at a specific rate or temperature below freezing point for ice crystal formation and growth throughout the solution. Then, the liquid slurry is subjected to freeze-drying to sublimate ice crystals under vacuum and leave behind void spaces resulting in an interconnected porous material matrix. Pore size, volume, and morphology are affected by variables such as freezing rate, temperature, solution concentration, solvent and solute types, and freezing direction [31]. Despite having good control of pore characteristics, freeze-drying limits the 3D architecture of the scaffold impeding the ability to create porosity at multiple length scales and precisely control scaffold geometry.

The particle leaching method incorporates soluble particles in a polymer solution such as sugars and salts to serve as pore-shaping agents and are then selectively removed in a solvent. Pore size, shape, and porosity of scaffolds are defined by the size, shape, and amount of particulates used [32]. However, precisely controlling pore interconnectivity is a major challenge with this technique. To address this, other techniques such as gas foaming are used in combination with particle leaching [33,34]. Gas foaming is a low-cost processing method which utilizes a blowing agent (i.e. chemical or physical) to create gas bubbles and produce porous polymeric structures [35]. This solvent-free technique can yield highly porous scaffolds but limitations include poor control of pore size and homogeneous

distribution of material which depends on the rheological properties of the polymer [36].

Electrospinning is a popular approach that is used to mimic the different fiber size ranges from the native extracellular matrix (ECM). In this method, a polymer solution is inserted from an electrically conductive nozzle to a collector with high voltage applied between the tip of the nozzle and the collector. The electric potential in the polymer solution overcomes surface tension forces creating a Taylor Cone. The polymer is ejected from the spinneret needle and is collected on the opposite end, resulting in a randomly oriented fibrous mesh ranging from 100 nm in diameter to a few microns [32]. The morphology of fibrous scaffolds formed can be modulated by changing the type of polymer, concentration, needle size, and voltage applied. However, the nature of the technique restricts the use of non-conductive materials and water-based solutions such as collagen whose surface tension forces are difficult to overcome [37]. Moreover, it has been previously shown that high voltages in this process denatures collagen, losing its chemical structure and superior biological properties [38].

3D printing has emerged as a significant additive manufacturing (AM) method in the tissue engineering field over the past decade [15]. The working principle of the method relies on layer-by-layer deposition of materials to build upon a three-dimensional scaffold. This method has provided significant advantages and addressed important drawbacks of conventional techniques such as the inability to

produce scaffolds with complex geometries, use multiple biomaterials simultaneously, as well as control porosity, pore size, and orientation [39,40]. Scaffolds can be custom designed through computer-aided design (CAD) software and built with 3D printing systems with precise porosity, architecture, and geometry.

2.3. 3D Printing for Tissue Engineering Applications

Commonly used 3D printing techniques for biomedical applications are broadly categorized into particle-fusion based methods, light-induced methods, inkjet printing, and extrusion-based printing [39]. Particle fusion-based 3D printing includes methods such as selective laser sintering (SLS), which use powders as the starting material. A CO_2 laser beam is traditionally used to raise the polymer temperature above melting point and fuse the particles together in the cross-sectional pattern of the 3D model to create a single layer. A new layer of particles is then laid over to repeat the process and build a layer-by-layer construct. Major limitations of this technique involve powder material wastage, limited printing resolution, and restricted use of biopolymers (i.e. synthetic polymers such as polycaprolactone (PCL), polyvinyl alcohol (PVA), and poly-L-lactic acid (PLLA)) [41,42]. Therefore, cell seeding efficiency is decreased due to reduced cell attachment and size disparity between cells and scaffold pore size.

Light-induced 3D printing techniques include stereolithography (SLA), which entails exposing a beam of UV light or laser onto a bath of photocurable liquid polymer and create gelled layers, constructing one on top of the other [39,43]. After gelling a single layer, the stage is moved to allocate a new layer of liquid polymer and repeat the process. SLA offers the advantage of a broad range of printing volume, high printing resolution, and good surface finish. However, despite the benefits, only a very limited range of biocompatible photocurable hydrogels are suitable for this technology. It may also require additional support structures to preserve the print fidelity and extensive post-curing processes [43]. Moreover, this method is typically applied to synthetic hydrogel polymer resins based on trimethylene carbonate (TMC), ε-caprolactone (CL), poly(propylene fumarate) (PPF), D,L-lactide (DLLA), and polyethylene glycol (PEG) [44,45].

Inkjet printing is a non-contact 3D printing technique that deposits droplets of ink in very small volumes (1-100 picolitres) onto a material bed [46]. Different types of inkjet-based printing are classified based on the state of the initial material bed which can be in powder or liquid form. A liquid binder is deposited on a powder bed, such as calcium phosphate, creating a cured 2D layer after which a new powder layer is spread and subsequently fused [47]. Uncured liquid materials are also used, such as alginic acid, and are gelled using a liquid crosslinker ink [48]. Overall, this 3D printing technique provides high controllability of drop-on-demand (DOD) deposition, high spatial resolution, and is especially useful in tissue engineering

applications [39,43]. Although a wider range of biomaterials can be used in inkjet 3D printing compared to the previously described methods, most require post-processing to clear constructs of unwanted material or binder residue in hollow spaces which is difficult to achieve.

Fused deposition modeling (FDM) is an extrusion-based 3D printing technique that utilizes a solid polymer in filament form that is extruded while being melted, typically at temperatures of up to 200 °C. These types of polymers require sharp transition between solid and melted states, where solidification must occur as the material is deposited and cooled to maintain its structure [49]. Thus, this technique requires materials with adequate thermal properties such as poly(lactic acid) (PLA), which makes this method unsuitable for most hydrogel inks. Applying high heat can cause thermal degradation, denaturation, and significantly decrease biocompatibility of hydrogels [43]. Therefore, an appropriate method to fabricate a wider variety of biocompatible hydrogel scaffolds and the most popular is direct extrusion 3D printing. Viscous hydrogel inks are loaded in a syringe and extruded through a needle in a continuous layering of microstrands. The strand thickness can be modified by changing the nozzle diameter, rate of deposition, and hydrogel viscosity. Nonetheless, the main drawback of this method is the lack of strength of some hydrogel inks to support their own weight and maintain their 3D structure and fidelity upon printing. Also, the printing resolution is limited and relatively low compared to particle-fusion based and light-induced 3D printing techniques [43].

2.4. Hydrogel Inks for Extrusion-Based 3D Printing

In extrusion-based 3D printing, hydrogel inks are used extensively in the tissue engineering field due to ease of use, versatility, and availability of an extensive variety of printable biomaterials [15]. Hydrogels are polymer matrices that mimic the natural ECM with properties such as porosity, high water content, appropriate biodegradation, and adjustable mechanical properties [50]. Moreover, hydrogels have the unique ability of directly loading cells at high densities, as well as bioactive molecules, and have shear-thinning properties that facilitate extrusion [15,16]. Consequently, they are highly promising biomaterials for extrusion 3D printing of cell-laden inks, also known as 3D bioprinting [51].

Commonly, hydrogel inks used for 3D printing derive from natural sources such as alginate [18], gelatin [52], cellulose [53], fibrinogen [54], hyaluronic acid (HA) [55], and collagen [56], or are made of synthetic polymers such as PEG, PCL [57], and gelatin methacrylamide (GelMA) [58]. Most 3D printed hydrogel constructs are weak and brittle, and usually lack the necessary sturdiness and desirable mechanical properties. To address this, natural and synthetic polymers are combined to form hydrogel-hydrogel composites and improve the mechanical stability while preserving biocompatibility of 3D printed constructs [43]. Multiple studies have reported the combination of different polymer inks to improve tensile

properties, toughness, swelling ratio, stiffness, and cell differentiation ability of 3D printed composite scaffolds [59–62].

Collagen type I is the most abundant extracellular matrix protein found in the human body and has been widely used as a promising biomimetic hydrogel bioink for 3D printing. Acid-solubilized collagen can be easily extruded and crosslinked *in situ* by replicating physiological temperature, pH, and ionic strength conditions, which makes it a suitable choice for 3D printing [63]. Furthermore, collagen possesses inherent cell attachment binding sites (i.e. RGD peptide sequences) that benefit cell adhesion and proliferation, unlike bioinks such as alginate which requires surface chemical modification [56]. It is evident that collagen possesses superior biological properties, benefits the function of certain cell types, and has high regenerative potential [64,65]. Yet, due to the weak mechanical properties of collagen, it has proved difficult to print collagen constructs and maintain their structural integrity using traditional 3D printing techniques.

2.5. FRESH 3D Printing

Freeform reversible embedding of suspended hydrogels, also known as FRESH, was first developed by Hinton et al. to address the challenges of printing soft hydrogel biomaterials [17]. To allow the precise deposition of hydrogels in

complex 3D structures and maintain their stability, a thermoreversible printing support bath composed of a secondary hydrogel was developed. The support bath is constituted of gelatin microparticles that behaves like a Bingham plastic, maintaining rigidity at low shear stresses and flowing as a liquid at high shear stresses. Hence, during the printing process, the support bath enables the free movement of a needle-like nozzle through the platform, while simultaneously holding the extruded hydrogel in its intended place. The printed hydrogel construct can then be recovered as the temperature is raised to a physiological temperature of 37 °C and the gelatin is melted and easily removed. Performed in sterile conditions, this is an ideal biocompatible environment to maintain viability of cell-laden bioprinting.

To produce FRESH, a solid block of gelatin is broken down into microparticles to form a slurry, with adaptable microparticle sizes depending on blending time. Previous works have shown the benefits of using FRESH 3D printing to ensure the stability of weak hydrogels such as collagen and alginate, improve print fidelity, and fabricate complex 3D structures that would have not been previously possible [14,18,66,67]. Hence, this technique has significantly amplified the versatility of 3D printing as a promising tissue engineering manufacturing technique.

2.6. Freeze-FRESH Methodology

Recently, Wang et al. reported a novel Freeze-FRESH (FF) 3D printing technique which combines freeze-casting and FRESH 3D printing to fabricate microporous alginate scaffolds [18]. The work aimed to fabricate scaffolds with hierarchical porosity, which proved difficult with the limited resolution of 3D printing capable of producing only macroscale pores by design. Thus, scaffolds were printed in FRESH support bath, frozen entirely within FRESH, lyophilized and consequently recovered from FRESH. In this way, the formation of microporosity with the construct struts was achieved and cell growth on the scaffolds was significantly enhanced. There are significant concerns with the negative impact of shear stresses on cell viability during extrusion [15,68], and thus incorporating microporosity on 3D printed scaffolds bypasses this issue.

Despite the advantages, different freezing temperatures of the FF technique (i.e. -20 °C and -80 °C) yielded alginate constructs with similar pore size, despite the ability of freezing temperature to modulate pore size [69]. The present work aimed to modify the FF methodology, use it to introduce microporosity with varying pore size in 3D printed collagen scaffolds, and asses the effects on material characteristics and cell response.

Chapter 3

Optimization of Freeze-FRESH Methodology for 3D Printing of Microporous Collagen Constructs

Abstract

Extrusion-based 3D bioprinting is a layer by layer technique that allows for the fabrication of custom-designed complex tissue architectures. However, suboptimal resolution of the extrusion printing technique offers little control over the microscopic features of the 3D construct. These microscopic features (e.g., pore size, pore morphology) are known to have a profound effect on cell migration, cell-cell interaction, proliferation, and differentiation. In a recent study, extrusion 3D printing via the Freeform reversible embedding of suspended hydrogels (FRESH) approach was combined with freeze-casting in the Freeze-FRESH (FF) method, which yielded alginate constructs with hierarchical porosity. However, use of the FF approach did not allow modulation of micropore size in the printed alginate constructs. In this study, the FF methodology was modified by melting the FRESH bath prior to freezing to allow more efficient heat transport and achieve greater control on the microporosity of the 3D printed collagen constructs. These modifications also allowed the collagen molecules to polymerize prior to freezing and thereby enable

printing of microporous collagen constructs using the FF methodology. The effects of different freezing temperatures on microporosity and physical properties of the 3D printed collagen constructs were assessed. Additionally, finite element (FE) models were generated to predict the mechanical properties of the porous constructs. Further, the impact of different micropore sizes on cellular response was evaluated. Freezing at lower temperature yielded constructs with smaller pore size. Compressive modulus of porous constructs was significantly lower than the non-porous control, and the FE model verified these findings. Constructs with larger micropore size were more stable. Cell metabolic activity and infiltration was enhanced in constructs with larger micropore size. Together, these results suggest that the FF method can be employed to guide the design of 3D printed microporous collagen constructs.

3.1 Introduction

Scaffold composition and architecture are key elements in the design of biomimetic tissue scaffolds. Use of natural biomaterials such as collagen is often preferred due to good biocompatibility, ease of processing, presence of cell binding sequences (i.e., RGD), and compositional biomimicry with native tissue [70,71]. Tissues are comprised of complex, highly organized hierarchical structures that range from nanoscale to macroscale that provide the characteristic tissue properties [72]. Therefore, scaffold microarchitecture, particularly at the cellular scale, is highly important and has been previously shown to govern cellular behavior, infiltration, differentiation, and nutrient exchange [4–7]. For example, collagen scaffolds with thicker fibers and larger pore sizes have been shown to increase secretion of proangiogenic factors and stimulate myofibroblastic differentiation of adipose stromal cells [73]. Further, collagen-based scaffolds with pore size greater than 325 microns have been shown to enhance cell infiltration and augment osteoblast differentiation and mineralization *in vitro* [7]. Therefore, biofabrication strategies that allow for the design and development of biomimetic tissue scaffolds with controlled microarchitecture are of paramount importance to guide cellular response and achieve functional tissue regeneration.

Freeze-casting and electrospinning are commonly employed to generate porous collagen scaffolds [30,32,74]; however, these methods are associated with significant limitations. The use of high voltage and corrosive solvents during the electrospinning process have raised concerns of collagen denaturation [38]. While freeze-casting is frequently used to generate porous collagen scaffolds without the use of organic solvents [75], scaffold geometry is constrained by the mold shape used for freezing the polymer solution [76]. Extrusion-based 3D printing allows for better spatial control over material deposition and hence is often implemented to generate porous scaffolds with complex geometries [77–80]. However, these printed scaffolds are devoid of microporous features below 100 microns due to limited resolution of the extrusion-based 3D printing technique [56,81]. Cell seeding onto extruded macroporous 3D printed constructs typically result in cell adhesion and population of the flat solid strut surfaces with limited cell infiltration to the core of the construct. Recent work using cellulose-based bioinks has shown that 3D printing can be combined with freeze-casting to fabricate microporous constructs [53,82]; however, this approach may not be directly applicable with collagen-based bioinks that need a support bath to provide structural support and aid in the polymerization of collagen molecules post printing which is essential for the generation of stable printed constructs. Further, these prior studies do not report on the efficiency of the combinatory approach to modulate the microporosity of the printed constructs.

Freeform reversible embedding of suspended hydrogels (FRESH) technique employs a thermoreversible gelatin support bath to enable layer by layer bioprinting of stable tissue constructs using soft hydrogel-based bioinks [17]. The ability to print complex structures such as heart components and patient-specific menisci using highly concentrated type I collagen bioinks (35 mg/ml) and the FRESH printing method has been previously demonstrated [14,83]. Lee et al. recently reported that incorporation of gelatin microparticles into collagen bioinks prior to printing and subsequent leaching of the microparticles post printing can yield collagen constructs with uniform microporosity [14]. Presence of microporosity can allow cell seeding and population of the construct after the printing process and thereby help circumvent concerns related to loss in shear-induced cell viability during the printing process. However, clogging of the extrusion needle by the microparticles during the printing process is a possible limitation [84]. Therefore, there is a need for alternative biofabrication methods to generate microporous collagen constructs to better control cell infiltration, cell-cell signaling, and nutrient transport, as well as improve cell proliferation and guide tissue-specific cell differentiation [85].

Recently, FRESH 3D printing was combined with freeze-casting in the Freeze-FRESH (FF) method to produce alginate constructs with hierarchical porosity [18]. This FF methodology involved 3D printing of alginate constructs in a support bath followed by freezing and lyophilization. However, the micropore size of the resulting constructs was comparable despite modulating the freezing temperature,

indicating that it was not feasible to modulate micropore size using different freezing temperatures with the FF technique. Herein, a modified FF printing technique is reported for the generation of microporous collagen constructs. The FF technique was modified by melting the gelatin support bath at 37 °C for 45 min prior to freezing to allow for better heat transfer via convective medium during the freezing process. Inclusion of the FRESH melting step also allowed gelation of the collagen prints which is essential for printing stable collagen constructs using the FF methodology. The micropore size was modulated by freezing the printed constructs in the melted gelatin support bath at -20 °C and -80 °C followed by lyophilization. The effect of different freezing temperatures on porosity, swelling, degradation, and mechanical properties of the 3D printed constructs was assessed. In addition, Saos-2 osteosarcoma cells were seeded onto 3D printed microporous constructs and the effect of pore size on cell morphology, infiltration, metabolic activity, and alkaline phosphatase (ALP) activity was investigated.

3.2 Materials and Methods

3.2.1 Preparation of Gelatin Slurry Support Bath

The gelatin support bath was prepared by adopting a protocol from previously published literature [17]. Briefly, 10 g of gelatin type A (Thermo Fisher Scientific, Waltham, MA) was added to 250 ml of 1x Phosphate Buffer Saline (PBS) in a 500 ml Mason jar, heated to 45 °C, and mixed until completely dissolved. The mix was then gelled at 4 °C for 24 h. Following this, chilled 1x PBS was added and filled to the brim of the gelatin containing jar and left to freeze at -20 °C for about 1 h. The frozen mixture was then blended in the same container at 20 second intervals for a total of 60 seconds using a household blender. The blended mixture was then transferred to 50 ml tubes and centrifuged at 3000 g for 5 min. The supernatant was discarded, and the tubes were filled with chilled 1x PBS and vortexed to resuspend the gelatin. The centrifugation step was repeated a few times to ensure complete removal of soluble gelatin. The individual tubes were then mixed to distribute the gelatin evenly and stored at 4 °C until use.

For 3D printing, the FRESH media was prepared by transferring two tubes of gelatin mixture into two 100 mL capped syringes and centrifuging at 180 g for 5 min. The supernatant was discarded and the mixture from one syringe was transferred to the other by extruding with a plunger to minimize the formation of bubbles. Air was

removed from the syringe and the syringe was centrifuged once again. The ready to use FRESH was then extruded into Petri dishes and stored at 4 °C.

3.2.2 3D Printing of Microporous Collagen Construct Using Freeze-FRESH Methodology

3D printed microporous collagen constructs (15 mm x 15 mm x 1 mm) were fabricated by adopting a previously published protocol on the FF methodology with modifications (Fig. 3.1) [18]. REGEMAT 3D (Granada, Spain) bioprinting system was used to print pure collagen constructs using highly concentrated neutralized type I collagen bioink (Lifeink® 200; 35 mg/ml; Advanced Biomatrix San Diego, CA) using the printing parameters outlined in Table 1. The collagen bioink was transferred using a coupler to a 3 ml syringe and centrifuged at 2000 rpm for 1 min to remove air bubbles. The capped syringe was then loaded onto the printer, and FRESH containing Petri dishes were placed onto the printer stage. The syringe cap was replaced with a 25G needle for extrusion and the printer was zeroed to begin printing in FRESH. Once printing was completed, constructs were incubated at 37 °C for 45 min to allow gelation of collagen as well as melting of the FRESH media. The printed constructs were then frozen at -20 °C (FF -20) or -80 °C (FF -80) within the melted FRESH media overnight. The frozen constructs were freeze dried in a lyophilizer (Labconco, Kansas City, MO) for 24 h. The constructs were then

recovered from the FRESH media by adding 1x PBS at room temperature and then incubated at 37 °C for about 45 min until the gelatin melted completely. The melted gelatin was removed by alternate washing of the constructs with deionized (DI) water and 1x PBS six times. Using a wide spatula, constructs were then carefully transferred to a new dish filled with DI water. The constructs were then frozen again at either -20 °C or -80 °C and subsequently lyophilized to obtain dry porous collagen constructs. Non-porous collagen constructs (control) were printed in a similar manner and recovered post FRESH melting without the freezing steps.

Table 3.1: Parameters for 3D printing of collagen constructs

Parameter	Value	Description
Tip Diameter	0.25 mm	A blunt syringe tip for the print head
Tip Gauge	25 g	
Print Shape	Cube	Outer limit of construct is square
Infill Pattern	Mesh	Inner pattern is cross hatched
Infill Angle	45°	The angle at which the bioink was extruded
Flow Speed	4 mm/s	Extrusion speed for optimal density

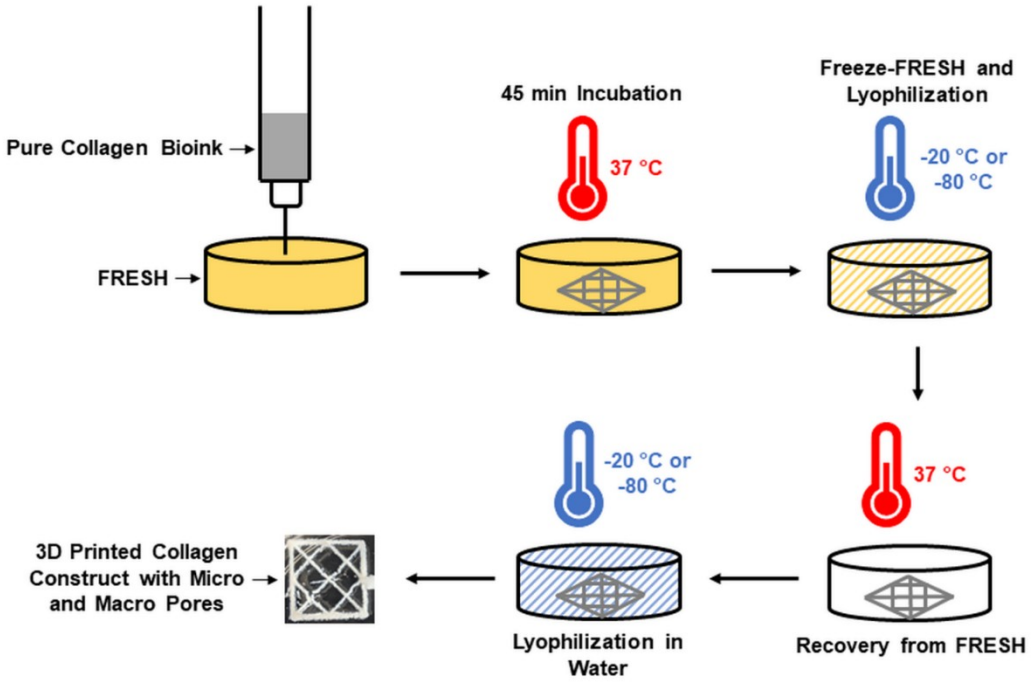

Figure 3.1: Schematic illustration of fabrication of 3D printed microporous collagen constructs using Freeze-FRESH methodology

3.2.3 Assessment of Microporosity of 3D Printed Collagen Constructs using SEM

Scanning Electron Microscopy (SEM) was used to assess the effect of different freezing temperatures on pore morphology (i.e., pore size, pore circularity, and pore size distribution) of the 3D printed collagen constructs (N = 4 constructs/group). Printed constructs were put on stubs, sputter coated with gold and imaged at 30x and 100x magnification with a JEOL JSM-6380LV SEM (JEOL, Tokyo, Japan). High magnification SEM images were analyzed using ImageJ to

measure pore size and pore circularity by calibrating the line measurement tool to the image scale (NIH, Bethesda, MD, USA). For pore size measurement, visible through-pores in the same focal plane were randomly chosen and measurements were manually performed using the line tool on 3 - 4 images per construct with a total of at least 150 measurements per group. The effective pore diameter (d) was obtained by using equation 1, where (l) is the pore long axis length and (s) is the pore short axis length [86]. All measurements were assembled to generate frequency histograms and assess pore size distribution. Pore circularity was measured using the freehand area selection tool in ImageJ and calculated using equation 2 from an extended version of the 'measure' command that calculates object circularity. A value of 1 indicates a perfect circle and a value of 0 indicates an elongated polygon.

$$d = \sqrt{l \times s} \tag{1}$$

$$Circularity = 4\pi \left(\frac{Area}{Perimeter^2} \right) \tag{2}$$

3.2.4 Assessment of Swelling Capacity of 3D Printed Microporous Collagen Constructs

Swelling studies were performed to determine the effect of different pore size on the degree of fluid absorption (N = 8/group). 3D printed porous constructs obtained by the FF method and non-porous control constructs were cut in half by using a sharp blade and weighed to measure the dry weight (W_d). Constructs were

then incubated in 500 µl of 1x PBS at room temperature for 24 h. Following this, constructs were removed from PBS using tweezers, blotted twice on a Kimwipe to remove the excess liquid, and placed onto an analytical balance to obtain the wet weight (W_w). The swelling degree was calculated as the percent change in weight to the initial dry weight as shown in equation 3.

$$Swelling\ Degree\ (\%) = \frac{W_w - W_d}{W_d} \times 100\% \quad (3)$$

3.2.5 Assessment of Stability of 3D Printed Microporous Collagen Constructs

An *in vitro* collagenase degradation assay was performed to assess the effect of different pore size on the stability of the 3D printed collagen constructs (N = 8/group). 3D printed constructs were hydrated with 1x PBS for 30 min prior to testing, blotted on a Kimwipe and weighed (W_o). Constructs were then incubated in 500 µl of the collagenase solution (5 U/ml in 0.1 M Tris-HCl buffer and 5 mM $CaCl_2$; pH 7.4) for 2 h at 37 °C under a constant stirring rate of 75 rpm. Constructs were then removed from solution, blotted on a Kimwipe and weighed again (W_f). The percent of residual mass post incubation was calculated using equation 4.

$$Residual\ Mass\ (\%) = \frac{W_f}{W_o} \times 100\% \quad (4)$$

3.2.6 Mechanical Characterization of 3D Printed Microporous Collagen Constructs

Compression tests were performed to assess the effect of different pore size on the compressive modulus of 3D printed collagen constructs (N = 4 constructs/group) by using an MT G2 MicroTester (CellScale Biomaterials Testing, Waterloo, Canada). Constructs were hydrated in 1x PBS, transferred to an acrylic platform, and placed into the testing chamber. A 0.3 mm diameter tungsten beam tipped with a 2 × 2 mm stainless-steel platen was used to compress the constructs. For each test, four measurements were taken per construct by applying a 10 μm/s loading rate until a 20% displacement of sample thickness was reached. The displacements at both the platen surface and the base of the tungsten beam were recorded. The compression force **P** extracted from the software is calculated using the Euler-Bernoulli beam theory shown in equation 5. In the equation, **δ** is the relative displacement of the platen to the base of the tungsten beam, **E** is the Young's modulus of the beam, **L** is the length of the beam, and **r** is the radius of the beam.

$$P = \frac{3\delta\, E\pi r^4}{4L^3} \tag{5}$$

Stress was computed by normalizing the load with the area of the compression platen and strain was determined by the ratio of **δ** to the original sample thickness. Stress–strain curves were generated, and the modulus was calculated as the slope of the stress–strain curve.

3.2.7 Finite Element Modeling of 3D printed Microporous Collagen Constructs

The compressive moduli of 3D printed collagen constructs were further investigated using FE models reconstructed from SEM images. ImageJ and an open source MATLAB code "Im2mesh" were used to convert SEM images into FE models for microporous collagen constructs [87,88]. The virtual compression of constructs was performed in the commercial code ABAQUS (Dassault Systemes Simulia Corp., Providence, RI). The Young's modulus of collagen was 1.71 kPa, obtained from the compression test of non-porous control samples. The modulus of liquid medium was 0.62 kPa. The Poisson's ratio for both constituents of the constructs was 0.3. A compression displacement of 10% was applied to the top surface of the constructs.

3.2.8 Cell Culture

Saos-2 human osteosarcoma cells (HTB-85, ATCC) where cultured in 75 cm^2 tissue culture flasks and maintained in Roswell Park Memorial Institute (RPMI) growth medium supplemented with 10% Fetal Bovine Serum (FBS), 1% L-glutamine, and 1% penicillin/streptomycin. Cells were expanded for 2 - 4 days at 37 °C and used for all the experiments. Printed constructs were sterilized in 70% ethanol for 30 min, transferred to an ultralow attachment 6-well plate (1 construct/well), and

washed with sterile 1x PBS. Saos-2 cells were seeded on top of the constructs at a density of 5,000 cells/cm^2 based on the area of the well (50,000 cells/well). The culture medium was replaced 6 hours post-seeding to remove unattached cells and the remaining adherent cells were cultured for 7 to 14 days. For assessment of cell metabolic activity and cell morphology, cells were maintained in Minimum Essential Medium Eagle - Alpha Modification (α-MEM) containing 10% FBS, 10 mM beta-glycerophosphate and 1% penicillin/streptomycin. For assessment of ALP activity, culture medium composed of α-MEM supplemented with 10% FBS, 10 mM beta-glycerophosphate, 10^{-7} M dexamethasone, and 1% penicillin/streptomycin. Culture medium was replaced every 3 days.

3.2.9 Assessment of Saos-2 Cell Metabolic Activity using Alamar Blue Assay

Alamar Blue (AB) assay was conducted to evaluate the effect of different pore size on cell metabolic activity (N = 8 constructs/group). The assay uses alamarBlue reagent which contains a non-toxic, cell-permeable, non-fluorescent blue indicator dye called resazurin. Upon penetrating living cells, resazurin is reduced in response to cellular metabolic activity into a highly fluorescent compound, resorufin, that is pink in color. Changes in cell metabolic activity can be easily detected with a fluorescence-based plate reader, where the intensity of the solution's fluorescence is proportional to the number of living cells. At periodic intervals (days 1, 4 and 7),

culture medium was replaced with a 10% solution of AB (Thermo Scientific) in α-MEM and incubated at 37 °C for 4 h. The same constructs were tested at each time point. Following this, 100 µL of AB solution was transferred in triplicate from each well into a separate 96-well plate. Fluorescence was measured using a SpectraMax M2e plate reader (Molecular Devices, San Jose, CA) with an excitation wavelength of 555 nm and emission wavelength of 595 nm.

3.2.10 Assessment of Saos-2 Cell Morphology and Infiltration on 3D Printed Microporous Collagen Constructs

Confocal microscopy (Nikon) was used to assess the effect of different pore size on Saos-2 cell morphology (N = 3 constructs/group/time point). At days 1 and 7, constructs were fixed with 3.7% formaldehyde solution (with 0.05% Triton X-100 in 1x PBS), washed twice with 1x PBS, and incubated in permeabilization buffer (0.1% Triton X-100 in 1x PBS). Then, constructs were washed twice with 1x PBS and incubated in blocking buffer (1% bovine serum albumin and 0.05% Triton X-100 in 1x PBS) for 30 min. Following this, constructs were washed with 1x PBS and stained with a working solution of AlexaFluor 488 phalloidin (1:25 dilution in 1x PBS) (Invitrogen, CA) for 30 min. The stain was then removed, and samples were washed twice with 1x PBS, wrapped in aluminum foil, and stored at 4 ºC prior to imaging. Cell infiltration into the collagen constructs was determined as the distance

between the highest and lowest point of visible cells in the z-axis, which is given by the thickness of the z-stack needed to capture the entire cell layers within the construct. Measurements were obtained from four images per construct for a total of at least 12 measurements per group.

3.2.11 Assessment of Alkaline Phosphatase Activity on 3D Printed Microporous Collagen Constructs

Alkaline Phosphatase (ALP) is an early biochemical marker for bone differentiation and is indicative of higher osteogenic activity when upregulated. To normalize ALP activity of Saos-2 cells, quantification of total amount of DNA was first performed using Quant-iT Picogreen dsDNA Kit (ThermoFisher Scientific) at days 7 and 14 (N = 3/group/time point). Saos-2 cells were cultured on 3D printed collagen constructs in α-MEM supplemented with 10% FBS, 1% penicillin/streptomycin, 10 mM beta-glycerophosphate, and 10^{-7} M dexamethasone (Sigma Aldrich). For cell harvest, collagen constructs were washed once with 1x PBS and incubated in 1 ml collagenase solution (1 mg/ml) mixed in a solution of 5 mM $CaCl_2$, 0.1 M HCl, and Trizma® base buffer pH 7.4 (Sigma Aldrich) at 37 °C with constant stirring of 75 rpm for 45 min to completely degrade the construct. Samples were then collected in microcentrifuge tubes and centrifuged at 2000 rpm for 5 min to obtain the cell pellet. Cells were lysed by adding 1x assay buffer to the

cell pellet in the microcentrifuge tubes. Then, 50 µl of cell lysates from each sample and equal volume of dsDNA reagent was added into each well of a 96-well plate in triplicate. The plate was then incubated at room temperature for 5 min covered from light with aluminum foil. Following incubation, fluorescence was measured at an excitation wavelength of 480 nm and emission wavelength of 520 nm using a SpectraMax M2e plate reader. DNA concentrations in cell lysates were obtained from a standard curve produced by using known concentrations of DNA.

ALP activity was measured at days 7 and 14 (N = 3/group/time point) using SensoLyte pNPP Alkaline Phosphatase Assay Kit (AnaSpec, Inc., Fremont, CA). A volume of 50 µl of the same cell lysates used for DNA quantification were added onto a separate 96-well plate along with an equal volume of pNPP solution in triplicate. Samples were incubated at room temperature for 60 min and absorbance was measured at 405 nm using a SpectraMax M2e plate reader. The ALP activity measured for each sample was normalized to the corresponding DNA content of Saos-2 cells to account for differences in cell number between constructs.

3.2.12 Statistical Analyses

Results are expressed as mean ± standard deviation. Data for SEM analyses, swelling study, and degradation assay was analyzed using one-way ANOVA followed by Tukey post-hoc test for pairwise comparisons (JMP Statistical

Discovery from SAS, Cary, NC). Statistical analysis for the mechanical characterization of collagen constructs was performed using MaxStat (MaxStat Software, Germany) with one-way ANOVA and Tukey post-hoc test. For the assessment of cell metabolic activity, cell infiltration, and ALP activity statistical analysis was performed using two-way ANOVA and Tukey post-hoc test (JMP). Statistical significance was set at $p < 0.05$.

3.3 Results

3.3.1 FF Method Allows Modulation of Micropore Size in 3D Printed Collagen Constructs

Assessment of SEM images revealed that the use of different FF freezing temperatures impacted the microporosity and pore size of 3D printed collagen constructs. 3D printed control constructs that were not subjected to freezing exhibited a solid non-porous surface morphology (Fig. 3.2A, D). SEM images of FF -80 constructs showed higher density of micropores and smaller pore size compared to FF -20 constructs (Fig. 3.2B, C, E, F). The average pore size of FF -20 constructs was 107 ± 56 μm, which was almost two-fold greater than FF -80 at 57 ± 23 μm (Table 2). Pore circularity, although statistically significant, was comparable between FF -20 and FF -80 constructs (Table 2). In addition, histograms for frequency-pore size distribution reveal a non-normal dataset for both FF -20 and FF -80 constructs (Fig. 3.2G, H). More importantly, FF -20 constructs showed greater spread in pore size distribution ranging from 28 - 346 μm compared to FF -80 which had values ranging from 18 - 132 μm. Together, these results indicate that it may be feasible to modulate the microporosity of 3D printed collagen constructs by modulating the freezing temperature during the FF fabrication process.

Table 3.2: Pore size and circularity of 3D printed collagen constructs (* indicates $p < 0.05$ when comparing between constructs with different micropore size)

Group	Pore Diameter (µm)	Circularity
FF -20	107 ± 56	0.776 ± 0.013
FF -80	57 ± 23*	0.801 ± 0.008*

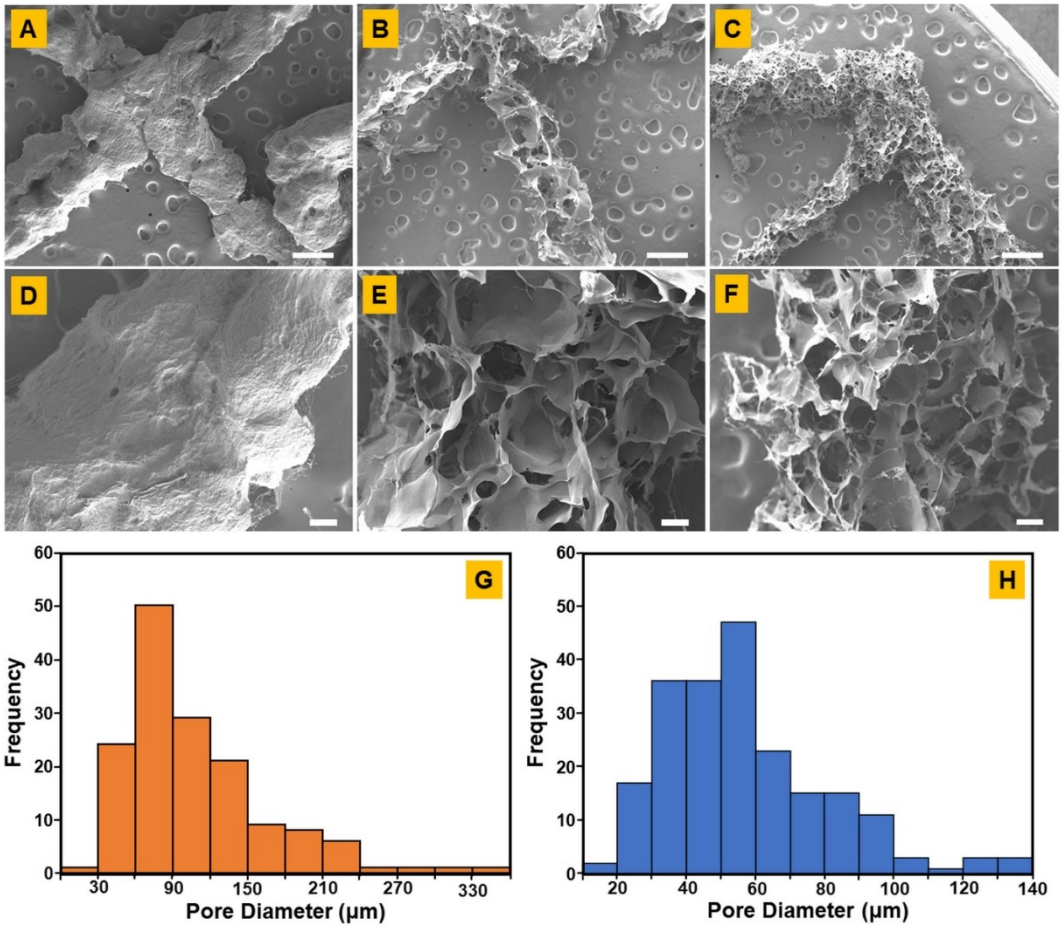

Figure 3.2: Assessment of microporosity in 3D printed collagen constructs fabricated using Freeze-FRESH methodology using SEM. Low and high magnification images of (A,D) non-porous control construct, (B, E) FF -20, (C, F) FF -80. Scale bar: 500 µm for (A-C) and 100 µm for (D-F). (G, H) Pore size distribution histograms for FF -20 constructs (G) and FF -80 (H).

3.3.2 Micropore Size Influences Stability of Collagen Constructs

In vitro swelling and degradation assays were performed to assess the effect of different pore sizes on fluid absorption and stability of 3D printed collagen constructs. Swelling degree is a measure of the percent increase in the weight of the construct due to fluid absorption. Control constructs were not used for swelling studies because they were not subjected to the freeze-drying process and hence were not prepared in the dry form. Swelling degree of FF -20 constructs and FF -80 constructs was comparable (Fig. 3.3A). Expectedly, the microporous 3D printed constructs degraded significantly faster than the non-porous control constructs (Fig. 3.3B). The residual mass of FF -80 constructs was 40%, which was significantly lower than FF -20 constructs at 56%, indicating that constructs with larger pore size were more stable. Together, these results suggest that the stability of 3D printed microporous constructs is influenced by the average pore size.

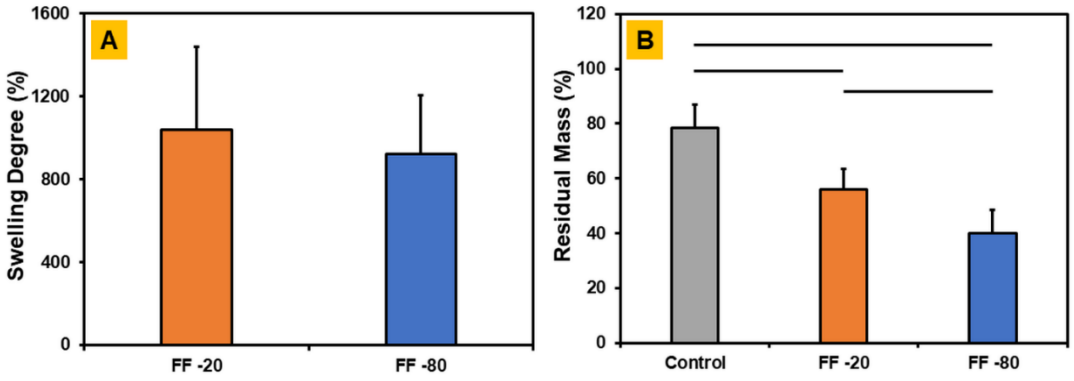

Figure 3.3: (A) Swelling degree, and (B) in vitro collagenase degradation of 3D printed microporous collagen constructs (horizontal line connecting groups denote $p < 0.05$).

3.3.3 Microporous Constructs Have Lower Compressive Modulus

Stress–strain curves obtained from compression testing of 3D printed collagen constructs are shown in Fig. 3.4A. The compressive modulus of the non-porous control constructs was at least two-fold higher than the microporous constructs (Fig. 3.4B). The compressive modulus of FF -20 constructs trended lower than FF -80 constructs indicating that larger the pore size lowered the stiffness of the construct (Fig. 3.4B). However, these results were not statistically significant. The average compressive moduli for control constructs and the FF -20 and FF -80 were found to be 1.71 ± 0.50 kPa, 0.69 ± 0.18 kPa and 0.87 ± 0.18 kPa, respectively.

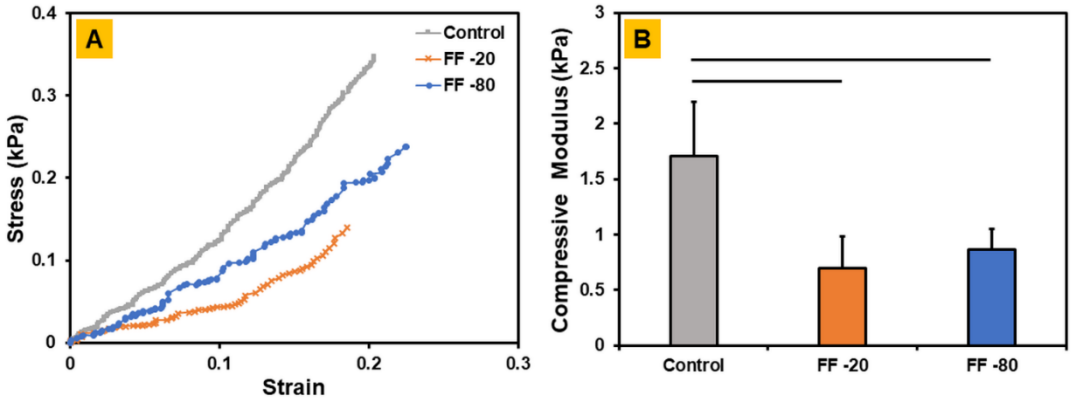

Figure 3.4: Mechanical assessment of 3D printed microporous collagen constructs. (A) Representative stress versus strain curves, and (B) Compressive modulus of 3D printed collagen constructs (horizontal line connecting groups denote $p < 0.05$).

3.3.4 FE Model Validates Experimental Data for Compressive Modulus

FE models reconstructed from the SEM images of 3D printed microporous collagen constructs were employed to assess compression induced stress and strain distributions in the constructs (Fig. 3.5A-L). Following compression, a uniform stress and strain were observed in the non-porous control construct, as expected. The compression stress of the control construct was 0.176 kPa at a compression strain of 0.1. On the other hand, the porous constructs demonstrated heterogeneous stress and strain distributions. The peak compressive stresses of the FF -20 and FF -80 were 0.245 kPa and 0.360 kPa, respectively. The peak compressive strain of the FF -20 and FF -80 were 0.011 and 0.030, respectively. It is worth noting that compression load led to the alignment of the collagen constructs that were associated with the directional trends in the stress and strain distributions. Specifically, the compressive stress distribution was directed along the loading direction, indicating the collagen elements carried the applied compression load. The compression strain distribution exhibited a directional trend perpendicular to the loading direction. These features might be used to guide the design of an anisotropic construct. In addition, the predicted compressive moduli from FE models agrees with experimental results with differences less than 5% (Fig. 3.5M).

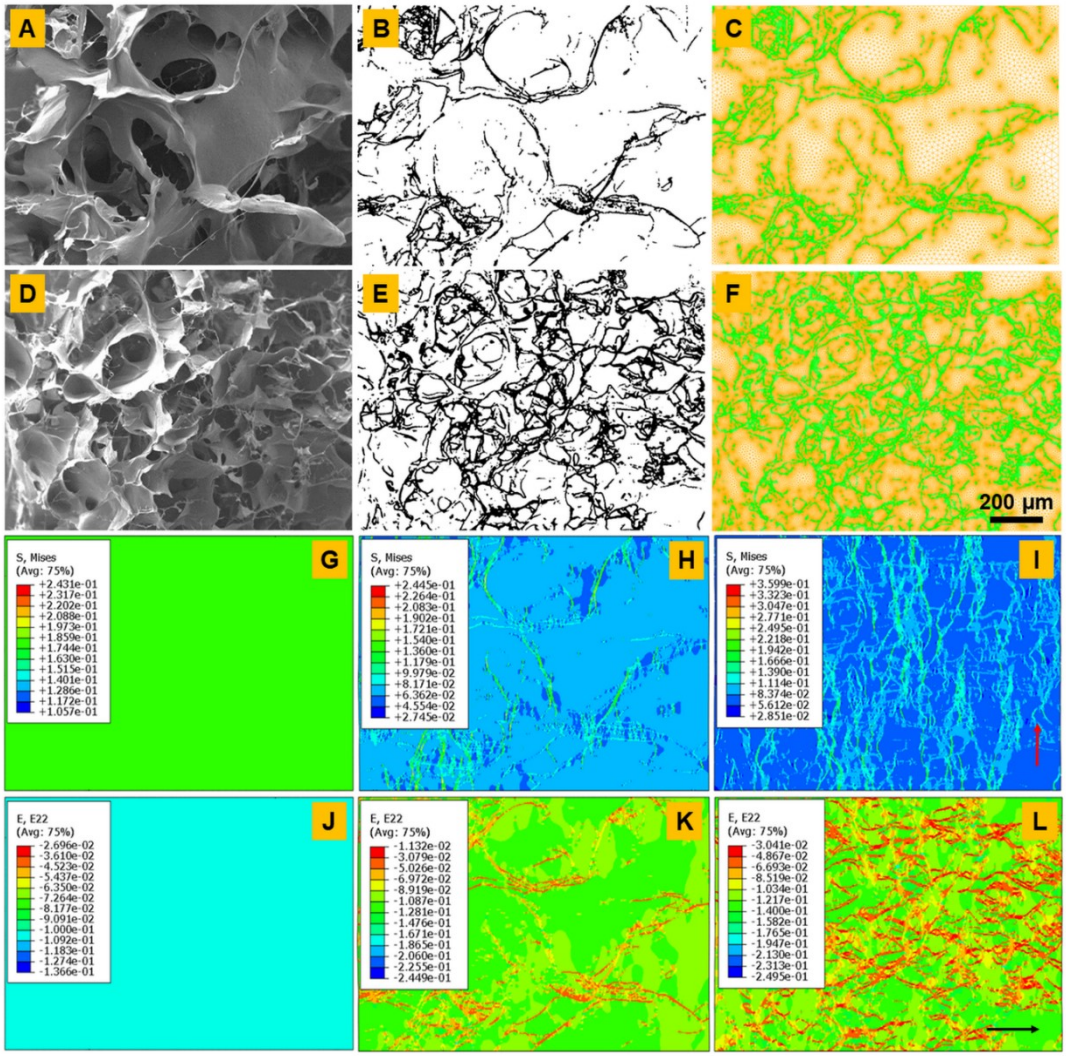

M

Group	Experiment (kPa)	Simulation (kPa)	Percent Difference (%)
Control	1.71	1.76	2.92
FF -20	0.69	0.71	2.90
FF -80	0.87	0.83	4.60

Figure 3.5: (A-F) Finite element model construction of 3D printed microporous collagen constructs. SEM images of FF -20 (A) and FF -80 (D), Image converting of respective SEM images (B, E), and finite element models (C, F). (G-L) Compression induced stress and strain distribution in nonporous control constructs (G, J), FF -20 (H, K) and FF -80 (I, L). (compression stress - (G-I) and compression strain - (J-L)).

(M) Experimental and estimated compression modulus of 3D printed collagen constructs.

3.3.5 Assessment of Saos-2 Cell Morphology on 3D Printed Microporous Collagen Constructs

Confocal imaging of stained cell cytoskeleton showed that cells exhibited a combination of round and spread morphology on all constructs indicating that the presence of micropores had no effect on cell morphology (Fig. 3.6). In addition, visible increase in cell number with time was observed on all constructs indicating that cells proliferated on microporous collagen constructs and non-porous controls. Cell infiltration depth at day 1 revealed that cell infiltration was significantly higher in FF -20 constructs compared to FF -80 constructs and non-porous controls (Fig. 3.7A). By day 7, cell infiltration was comparable for all groups. Together, these results suggest that larger pore size allows better early cell infiltration in 3D printed microporous collagen constructs.

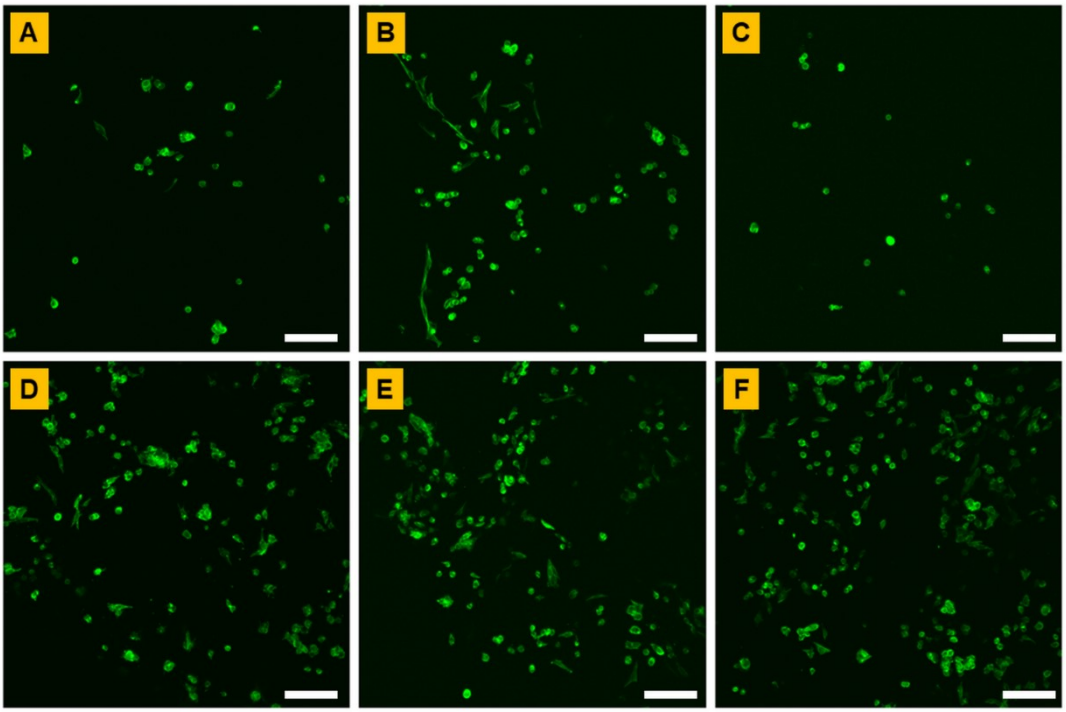

Figure 3.6: Assessment of cell morphology via cytoskeleton staining using Alexa Fluor 488 Phalloidin. (A-C) Day 1 for (A) non-porous control construct, (B) FF -20 and (C) FF -80. (D-F) Day 7 for (D) non-porous control construct, (E) FF -20, and (F) FF -80. Scale bar: 100 µm.

3.3.6 Micropores Improve Cell Infiltration and Metabolic Activity of Saos-2 Cells

Saos-2 cells were cultured on FF constructs and non-porous control constructs to quantify the effect of pore size on cell metabolic activity using an AB assay. Results showed that cell metabolic activity increased with time on all constructs. Specifically, cell metabolic activity was significantly different at all time points on FF -20 and FF -80, and significantly different between day 1 and day 7 for

the non-porous collagen constructs (Fig. 3.7B). The FF -20 constructs exhibited significantly greater cell metabolic activity compared to control at day 4 and day 7, and FF -80 constructs showed significantly higher cell metabolic activity compared to control at day 7. Cell metabolic activity trended higher on FF -20 constructs compared to FF -80 at all time points, although these results were not statistically significant. Together, results from the AB assay suggest that the presence of micropores enhances cell metabolic activity.

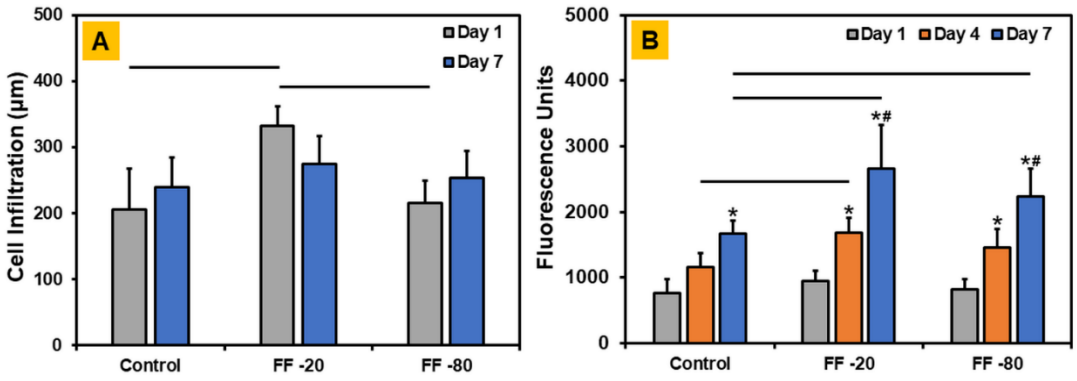

Figure 3.7: (A) Cell infiltration, and (B) cell metabolic activity on 3D printed microporous collagen constructs (horizontal line denotes $p < 0.05$ when comparing between constructs at the same time point, * indicates $p < 0.05$ when comparing with day 1, and # indicates $p < 0.05$ when comparing with day 4).

3.3.7 Assessment of Saos-2 Cell Alkaline Phosphatase Activity

ALP activity was comparable on all constructs at day 7 followed by a significant decrease from day 7 to day 14 (Fig. 3.8). At day 14, FF -80 constructs

showed significantly lower ALP activity compared to control. Similarly, lower ALP activity was also observed on FF -20 constructs compared to control but this difference was not statistically significant ($p = 0.16$). ALP activity was similar at both time points for the two FF constructs. Together, these results suggest that ALP activity in Saos-2 cells may decrease upon introduction of microporosity in 3D printed collagen constructs and that the size of the micropores had no effect on ALP activity.

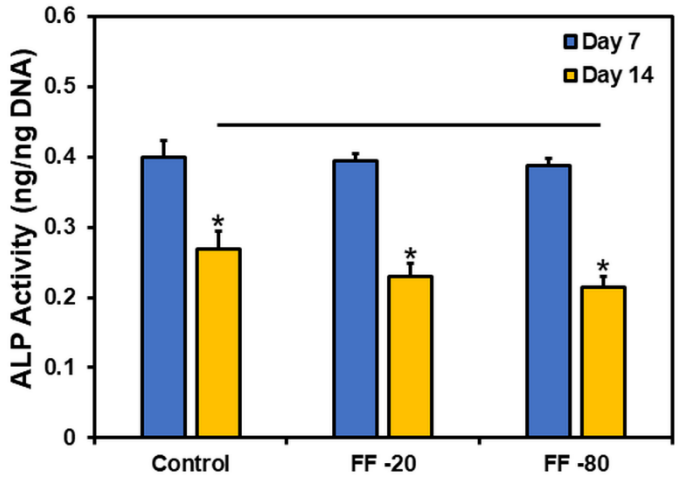

Figure 3.8: Assessment of ALP activity on 3D printed microporous collagen constructs (horizontal line connecting groups denote $p < 0.05$, and * indicates $p < 0.05$ when comparing with day 7).

3.4 Discussion

Application of the FF technique with alginate bioinks has been shown to yield 3D printed constructs with hierarchical porosity [18]. Adoption of the same protocol to generate collagenous constructs is not feasible because freezing the construct in the support bath immediately after printing does not allow the collagen molecules to polymerize. Therefore, the resulting construct is unstable and does not survive the subsequent steps in the process. The modified FF technique employed in the current study entailed incubation of the construct in the FRESH bath after the printing process at 37 °C for 45 min to allow for the collagen molecules to polymerize, undergoing fibrillogenesis and form a stable 3D construct (Fig. 3.1). Incubation at 37 °C also melts the FRESH bath into a liquid medium. This simple modification to the FF technique may have allowed better heat transfer to occur during the subsequent ice templating process yielding 3D printed constructs with more controlled microporosity. Microporous structures generated from freeze-casting are governed by the rate of heat transfer during freezing and the final freezing temperature of the substrate [89]. The rate of heat transfer controls the number of ice crystal nucleation sites formed (i.e., number of pores), and the rate of heat diffusion away from the nucleation points determines the size of ice crystals (i.e., size of the pores) [11]. The final freezing temperature, the height of solidified fluid layer, and the thermal properties of the suspension in both liquid and solid state regulate the

velocity of solidification [76]. Prior work with FF technique and alginate bioinks did not achieve similar control over the porosity of the printed constructs as in the current study because the freezing step was performed with the support bath in a solidified state resulting in comparable rates of heat transfer despite changing the freezing temperature. Attainment of greater control of microporosity in 3D printed constructs is significant and can be leveraged for the fabrication of tissue-specific scaffolds for different biomedical applications such as bone and skin regeneration.

In the conventional freeze-casting process, the size and orientation of the micropores can be controlled by modulating the freezing temperature and directionality of freezing [22,74]. Results from this study are in accordance with previous literature and showed that freezing the constructs with the melted FRESH bath at -80 ºC yielded constructs with significantly smaller micropores compared to the constructs frozen at -20 ºC (Fig. 3.2). Further, FF -80 constructs exhibited a homogenous porous structure as evidenced by a more uniform pore size compared to FF -20 constructs (Table 2). Similar outcomes in terms of micropore size distribution were previously reported using collagen/PCL scaffolds [90]. Lower freezing temperatures create a larger temperature difference between the freezing source and the solution freezing temperature, resulting in expedited nucleation of ice crystals followed by a limited crystal growth phase, thereby producing smaller, more uniform micropores [11,86]. On the other hand, freezing constructs at higher temperatures results in a more prolonged crystal growth phase, which in turn, causes

more variability in micropore size and morphology yielding scaffolds with broader pore size distribution.

Typically, scaffolds with larger pore size are expected to allow for greater fluid permeability and nutrient flow [69]. Swelling results in the current work indicated that printed collagen FF constructs with different micropore size yielded similar swelling properties (Fig. 3.3A). These results are consistent with a previous study that showed that swelling properties of freeze-dried recombinant human collagen peptide-chitosan scaffolds are independent of the micropore size [86]. In a separate study, the swelling and degradation properties of freeze-dried collagen/hyaluronan/chitosan scaffolds were reported to decrease with decreased scaffold pore size due to reduced penetration of the fluid or enzyme solution resulting in slower scaffold degradation [91]. Contrary to this outcome, the current study indicated that constructs with smaller pore size degraded faster possibly due to thinner pore walls (Fig. 3.3B). Since all three scaffold types were printed with the same amount of material, variations in pore size will have an impact on pore wall thickness. Further, it has been previously documented that pore size and specific surface area have an inverse relationship [69], which can explain the significantly faster degradation of collagen constructs with smaller pore size and higher surface area. Together, these results suggest that by controlling the micropore size, it is feasible to maintain the fluid uptake properties while modulating the degradation properties of the 3D printed microporous collagen constructs.

Assessment of mechanical properties showed the compressive modulus of collagen constructs with different micropore size was comparable (Fig.4). This could be attributed to load sharing capacity of the liquid medium within the constructs, as the effective modulus of liquid medium is approximately one third of the collagen modulus. Smooth nonporous control constructs showed significantly higher stiffness compared to FF -20 and FF-80 porous constructs. These results are in agreement with previous work on microporous alginate scaffolds using the FF technique [18]. Similar results have also been shown with collagen-based scaffolds wherein change in average micropore size from 96 to 151 μm had no impact on the compressive modulus of the scaffolds [92]. In addition, FE models captured the local compressive mechanics of the constructs and showed heterogeneous stress and strain distributions in porous collagen constructs (Fig. 5). Compared with the control group, the porous constructs exhibited larger stresses and lower strains because of the presence of the liquid medium in the micro porosities (Fig. 5G-5L). The FF -20 constructs showed much lower strain compared to FF -80 constructs which is indicative of increased resistance to the compression load due to the larger volume fraction of the liquid medium in the FF -20 constructs (Fig. 5K, 5L). Results also demonstrated the compression induced alignment of the porous collagen constructs as well as the directional trends in their stress and strain distributions. This observation could be leveraged to guide the design of novel constructs with regulated directional modulus.

Moreover, virtual experiments using FE models might enable the optimization of porous constructs for the enhanced mechanical environment of cells [93].

Scaffold microstructural features play an essential role in regulating cell behavior and fate [23,73,94]. Confocal imaging of Saos-2 cells seeded on 3D printed collagen constructs revealed that cell morphology was maintained with no visible differences on both non-porous control and porous constructs (Fig. 3.6). Quantitative analyses revealed significantly higher cell infiltration on FF -20 constructs with larger pore size at day 1 (Fig. 3.7A) indicating greater cell migration into the construct which may be a viable cell population strategy. By day 7, cell infiltration was found to be comparable between constructs which may be attributed to initial cell-mediated remodeling of the uncrosslinked collagen construct. AB results showed significantly greater cell metabolic activity and proliferation on porous constructs compared to control, possibly due to the greater surface area to better support cell attachment and growth (Fig. 3.7B). These results are in agreement with prior work that show enhanced cell infiltration and proliferation on collagen scaffolds with larger pore size [22]. Osteoblasts need to be in dense layers to differentiate and mineralize. Preliminary work to assess Saos-2 cell differentiation showed lower ALP activity on porous constructs compared to the non-porous control (Fig. 3.8). It is likely that the availability of higher surface area in microporous collagen constructs resulted in a prolonged proliferative phase and delayed onset of cell differentiation. Further, lower ALP activity on porous constructs may also be

attributed to the lower stiffness of porous constructs compared to non-porous controls [95].

In conclusion, results from the current study demonstrate that the modified FF method can be reliably employed to 3D print microporous collagen constructs. Further, the microporosity of 3D printed collagen constructs can be modulated by employing different freezing temperatures. Introduction of microporosity via the modified FF approach decreased mechanical properties, expedited degradation, and enhanced cell infiltration and proliferation in 3D printed collagen constructs. Further, FE model developed in this work allows to predict the effect of microporosity on the mechanical properties of the collagen constructs. Future studies will entail performing longer-term cultures and employing mesenchymal stem cells (MSCs) to assess the effects of microporosity on cell functionality such as osteogenic differentiation and vascularization.

Acknowledgements

This work is supported in part by a grant from the NIH (1R15AR071102). The authors would like to thank Ms. Gayle Duncombe for her help with SEM and Mr. Trevor Schmitt for his help with 3D printing and preparation of FRESH support media.

Chapter 4

Conclusions and Future Work

4.1 Summary and Conclusions

The fabrication of biomimetic 3D printed collagen constructs was possible as a result of modifying and optimizing the FF methodology. Different freezing temperatures (i.e. -20 °C and -80 °C) were able to modulate the microporosity and pore size incorporated in the struts of 3D printed constructs. A lower temperature of -80 °C yielded constructs with smaller micropores (FF -80) compared to constructs frozen at -20 °C (FF -20). Assessment of swelling degree revealed that both microporous constructs frozen at different temperatures had comparable fluid absorption. However, FF -80 constructs with smaller micropore size degraded significantly faster than FF -20 constructs, and predictably, both degraded faster than non-porous controls. Likewise, both microporous constructs had lower compressive moduli than non-porous constructs, with FF -20 trending lower than FF -80, but not sufficient to be statistically significant. FE models developed from SEM micrographs were able to successfully predict experimental results with differences of less than 5%. The presence of micropores on collagen constructs did not affect Saos-2 cell morphology, yet an increased cell proliferation was observed on microporous collagen constructs compared to control. Cell infiltration was also enhanced on constructs with larger micropore size (FF -20) on the initial period of cell culture.

Finally, ALP activity of Saos-2 cells was comparable at day 7 on all constructs with FF -80 showing a decrease at day 14 with lower values compared to control, suggesting that microporosity may decrease cell ALP activity. Together, results from this work show that the FF method can be effectively used to fabricate microporous 3D printed collagen constructs. Micropore size and degradation can also be modulated by changing the freezing temperature the FF method to create an impact in cell metabolic activity and infiltration.

4.2 Future Work

Although the present work achieved the optimization of the FF fabrication method to yield microporous biomimetic scaffolds, several areas have been identified for further research and future directions of the current project. Firstly, introducing the step of melting FRESH at 37 °C prior to the freeze-drying cycle allowed different freezing temperatures to control micropore size of collagen constructs. An in-depth investigation would be necessary to understand the influence of material state on the underlying heat transfer mechanisms of the FF technique. Presently, it is evident that the solid or liquid state of the FRESH media affects the ability to control micropore size of 3D printed constructs, but the mechanism by which this occurs is not yet understood.

Secondly, this project used Saos-2 human osteosarcoma cell line as a model to study the effect of microporosity on cell behavior. The effect of microporosity can be further investigated on tissue-specific cellular response such as the mineralization of Saos-2 cells or the osteogenic differentiation of human mesenchymal stem cells (hMSCs). To achieve this, quantitative assays such as calcium quantification and real-time PCR can be performed, respectively. Lastly, angiogenesis is essential for successful tissue engineering scaffolds. A network of blood vessels is vital for constructs to survive and allow integration with surrounding tissue [96]. Thus, the angiogenic potential of 3D printed collagen scaffolds could be investigated used *in vitro* tests to evaluate the ability of constructs to benefit endothelial cell adhesion, growth, and performance. A co-culture of endothelial cells (ECs) and osteoblasts can be conducted *in vitro* to assess the formation of neo-angiogenesis; previous work by Unger et al. observed microcapillary-like structures in three-dimensional constructs with co-culture of ECs and osteoblasts only [97].

References

[1] A. Persidis, Biotechnology 2000, Nat. Biotechnol. 17 (1999) 1239–1239. https://doi.org/10.1038/70809.

[2] F.J. O'Brien, Biomaterials & Scaffolds for Tissue Engineering, Mater. Today. 14 (2011) 88–95. https://doi.org/10.1016/S1369-7021(11)70058-X.

[3] R. Lanza, R. Langer, J.P. Vacanti, A. Atala, Principles of Tissue Engineering, 5th ed., Academic Press, 2020, 2020. https://books.google.com/books?id=Fz_ZDwAAQBAJ.

[4] Z. Liu, M. Tamaddon, Y. Gu, J. Yu, N. Xu, F. Gang, X. Sun, C. Liu, Cell Seeding Process Experiment and Simulation on Three-Dimensional Polyhedron and Cross-Link Design Scaffolds, Front. Bioeng. Biotechnol. 8 (2020). https://doi.org/10.3389/fbioe.2020.00104.

[5] R.A. Perez, G. Mestres, Role of pore size and morphology in musculo-skeletal tissue regeneration, Mater. Sci. Eng. C. 61 (2016) 922–939. https://doi.org/10.1016/j.msec.2015.12.087.

[6] H.P. Dang, C. Vaquette, T. Shabab, R.A. Pérez, Y. Yang, T.R. Dargaville, A. Shafiee, P.A. Tran, Porous 3D Printed Scaffolds For Guided Bone Regeneration In a Rat Calvarial Defect Model, Appl. Mater. Today. 20 (2020) 100706. https://doi.org/10.1016/j.apmt.2020.100706.

[7] C.M. Murphy, G.P. Duffy, A. Schindeler, F.J. O'Brien, Effect of collagen-glycosaminoglycan scaffold pore size on matrix mineralization and cellular behavior in different cell types, J. Biomed. Mater. Res. - Part A. (2016). https://doi.org/10.1002/jbm.a.35567.

[8] J. Zhu, R.E. Marchant, Design properties of hydrogel tissue-engineering scaffolds, Expert Rev. Med. Devices. 8 (2011) 607–626. https://doi.org/10.1586/erd.11.27.

[9] C.H. Lee, A. Singla, Y. Lee, Biomedical applications of collagen, Int. J. Pharm. 221 (2001) 1–22. https://doi.org/10.1016/S0378-5173(01)00691-3.

[10] Z.-L. Mou, L.-M. Duan, X.-N. Qi, Z.-Q. Zhang, Preparation of silk fibroin/collagen/hydroxyapatite composite scaffold by particulate leaching method, Mater. Lett. 105 (2013) 189–191. https://doi.org/10.1016/j.matlet.2013.03.130.

[11] F.J. O'Brien, B.A. Harley, I. V. Yannas, L. Gibson, Influence of freezing rate on pore structure in freeze-dried collagen-GAG scaffolds, Biomaterials. (2004). https://doi.org/10.1016/S0142-9612(03)00630-6.

[12] J.A. Matthews, G.E. Wnek, D.G. Simpson, G.L. Bowlin, Electrospinning of collagen nanofibers, Biomacromolecules. (2002). https://doi.org/10.1021/bm015533u.

[13] V. Kishore, W. Bullock, X. Sun, W.S. Van Dyke, O. Akkus, Tenogenic differentiation of human MSCs induced by the topography of electrochemically aligned collagen threads, Biomaterials. 33 (2012) 2137–2144. https://doi.org/10.1016/j.biomaterials.2011.11.066.

[14] A. Lee, A.R. Hudson, D.J. Shiwarski, J.W. Tashman, T.J. Hinton, S. Yerneni, J.M. Bliley, P.G. Campbell, A.W. Feinberg, 3D bioprinting of collagen to rebuild components of the human heart, Science (80-.). 365 (2019) 482–487. https://doi.org/10.1126/science.aav9051.

[15] J.K. Placone, A.J. Engler, Recent Advances in Extrusion-Based 3D Printing for Biomedical Applications, Adv. Healthc. Mater. 7 (2018) 1701161. https://doi.org/10.1002/adhm.201701161.

[16] C. Xu, G. Dai, Y. Hong, Recent advances in high-strength and elastic hydrogels for 3D printing in biomedical applications, Acta Biomater. (2019). https://doi.org/10.1016/j.actbio.2019.05.032.

[17] T.J. Hinton, Q. Jallerat, R.N. Palchesko, J.H. Park, M.S. Grodzicki, H.-J. Shue, M.H. Ramadan, A.R. Hudson, A.W. Feinberg, Three-dimensional printing of complex biological structures by freeform reversible embedding of suspended hydrogels, Sci. Adv. 1 (2015) e1500758. https://doi.org/10.1126/sciadv.1500758.

[18] Z. Wang, S.J. Florczyk, Freeze-FRESH: A 3D Printing Technique to Produce Biomaterial Scaffolds with Hierarchical Porosity, Materials (Basel). 13 (2020) 354. https://doi.org/10.3390/ma13020354.

[19] E.L. De Mulder, P. Buma, G. Hannink, Anisotropic Porous Biodegradable Scaffolds for Musculoskeletal Tissue Engineering, Materials (Basel). 2 (2009) 1674–1696. https://doi.org/10.3390/ma2041674.

[20] S.J. Hollister, Porous scaffold design for tissue engineering, Nat. Mater. 4 (2005) 518–524. https://doi.org/10.1038/nmat1421.

[21] F.J. O'Brien, B.A. Harley, I. V. Yannas, L.J. Gibson, The effect of pore size on cell adhesion in collagen-GAG scaffolds, Biomaterials. (2005). https://doi.org/10.1016/j.biomaterials.2004.02.052.

[22] C.M. Murphy, M.G. Haugh, F.J. O'Brien, The effect of mean pore size on cell attachment, proliferation and migration in collagen–glycosaminoglycan scaffolds for bone tissue engineering, Biomaterials. 31 (2010) 461–466. https://doi.org/10.1016/j.biomaterials.2009.09.063.

[23] C.M. Murphy, F.J. O'Brien, Understanding the effect of mean pore size on cell activity in collagen-glycosaminoglycan scaffolds, Cell Adhes. Migr. (2010). https://doi.org/10.4161/cam.4.3.11747.

[24] A. Phadke, Y. Hwang, S.H. Kim, S.H. Kim, T. Yamaguchi, K. Masuda, S. Varghese, Effect of scaffold microarchitecture on osteogenic differentiation of human mesenchymal stem cells., Eur. Cell. Mater. 25 (2013) 114–129. https://doi.org/10.22203/ecm.v025a08.

[25] Q. Fu, M.N. Rahaman, B.S. Bal, R.F. Brown, In vitro cellular response to hydroxyapatite scaffolds with oriented pore architectures, Mater. Sci. Eng. C. 29 (2009) 2147–2153. https://doi.org/10.1016/j.msec.2009.04.016.

[26] M.J. Gupte, W.B. Swanson, J. Hu, X. Jin, H. Ma, Z. Zhang, Z. Liu, K. Feng, G. Feng, G. Xiao, N. Hatch, Y. Mishina, P.X. Ma, Pore size directs bone marrow stromal cell fate and tissue regeneration in nanofibrous macroporous scaffolds by mediating vascularization, Acta Biomater. 82 (2018) 1–11. https://doi.org/10.1016/j.actbio.2018.10.016.

[27] G. Hannink, J.J.C. Arts, Bioresorbability, porosity and mechanical strength of bone substitutes: What is optimal for bone regeneration?, Injury. 42 (2011) S22–S25. https://doi.org/10.1016/j.injury.2011.06.008.

[28] D. Yoo, New paradigms in hierarchical porous scaffold design for tissue engineering, Mater. Sci. Eng. C. 33 (2013) 1759–1772. https://doi.org/10.1016/j.msec.2012.12.092.

[29] S.S. Liao, F.Z. Cui, W. Zhang, Q.L. Feng, Hierarchically biomimetic bone scaffold materials: Nano-HA/collagen/PLA composite, J. Biomed. Mater. Res. 69B (2004) 158–165. https://doi.org/10.1002/jbm.b.20035.

[30] M. Kim, Y.E. Choe, G.H. Kim, Injectable hierarchical micro/nanofibrous collagen-based scaffolds, Chem. Eng. J. (2019). https://doi.org/10.1016/j.cej.2019.02.044.

[31] L. Qian, H. Zhang, Controlled freezing and freeze drying: A versatile route for porous and micro-/nano-structured materials, J. Chem. Technol. Biotechnol. (2011). https://doi.org/10.1002/jctb.2495.

[32] E. Babaie, S.B. Bhaduri, Fabrication Aspects of Porous Biomaterials in Orthopedic Applications: A Review, ACS Biomater. Sci. Eng. 4 (2018) 1–39. https://doi.org/10.1021/acsbiomaterials.7b00615.

[33] Y.S. Nam, J.J. Yoon, T.G. Park, A novel fabrication method of macroporous biodegradable polymer scaffolds using gas foaming salt as a porogen additive, J. Biomed. Mater. Res. (2000). https://doi.org/10.1002/(SICI)1097-4636(2000)53:1<1::AID-JBM1>3.0.CO;2-R.

[34] L.D. Harris, B.S. Kim, D.J. Mooney, Open pore biodegradable matrices formed with gas foaming, J. Biomed. Mater. Res. (1998). https://doi.org/10.1002/(SICI)1097-4636(19981205)42:3<396::AID-JBM7>3.0.CO;2-E.

[35] I. Manavitehrani, T.Y.L. Le, S. Daly, Y. Wang, P.K. Maitz, A. Schindeler, F. Dehghani, Formation of porous biodegradable scaffolds based on poly(propylene carbonate) using gas foaming technology, Mater. Sci. Eng. C. 96 (2019) 824–830. https://doi.org/10.1016/j.msec.2018.11.088.

[36] V. Santos-Rosales, A. Iglesias-Mejuto, C.A. García-González, Solvent-Free Approaches for the Processing of Scaffolds in Regenerative Medicine, Polymers (Basel). 12 (2020) 533. https://doi.org/10.3390/polym12030533.

[37] K. Sarkar, C. Gomez, S. Zambrano, M. Ramirez, E. De Hoyos, H. Vasquez, K. Lozano, Electrospinning to Forcespinning™, Mater. Today. (2010). https://doi.org/10.1016/S1369-7021(10)70199-1.

[38] D.I. Zeugolis, S.T. Khew, E.S.Y. Yew, A.K. Ekaputra, Y.W. Tong, L.-Y.L. Yung, D.W. Hutmacher, C. Sheppard, M. Raghunath, Electro-spinning of pure collagen nano-fibres – Just an expensive way to make gelatin?, Biomaterials. 29 (2008) 2293–2305. https://doi.org/10.1016/j.biomaterials.2008.02.009.

[39] M. Guvendiren, J. Molde, R.M.D. Soares, J. Kohn, Designing Biomaterials for 3D Printing, ACS Biomater. Sci. Eng. 2 (2016) 1679–1693. https://doi.org/10.1021/acsbiomaterials.6b00121.

[40] U. Jammalamadaka, K. Tappa, Recent advances in biomaterials for 3D printing and tissue engineering, J. Funct. Biomater. (2018). https://doi.org/10.3390/jfb9010022.

[41] J. An, J.E.M. Teoh, R. Suntornnond, C.K. Chua, Design and 3D Printing of Scaffolds and Tissues, Engineering. (2015). https://doi.org/10.15302/J-ENG-2015061.

[42] S.F.S. Shirazi, S. Gharehkhani, M. Mehrali, H. Yarmand, H.S.C. Metselaar, N. Adib Kadri, N.A.A. Osman, A review on powder-based additive manufacturing for tissue engineering: Selective laser sintering and inkjet 3D printing, Sci. Technol. Adv. Mater. (2015). https://doi.org/10.1088/1468-6996/16/3/033502.

[43] T.-S. Jang, H.-D. Jung, H.M. Pan, W.T. Han, S. Chen, J. Song, 3D printing of hydrogel composite systems: Recent advances in technology for tissue engineering, Int. J. Bioprinting. 4 (2018). https://doi.org/10.18063/ijb.v4i1.126.

[44] F.P.W. Melchels, J. Feijen, D.W. Grijpma, A review on stereolithography and its applications in biomedical engineering, Biomaterials. (2010). https://doi.org/10.1016/j.biomaterials.2010.04.050.

[45] T.M. Seck, F.P.W. Melchels, J. Feijen, D.W. Grijpma, Designed biodegradable hydrogel structures prepared by stereolithography using poly(ethylene glycol)/poly(d,l -lactide)-based resins, J. Control. Release. 148 (2010) 34–41. https://doi.org/10.1016/j.jconrel.2010.07.111.

[46] B. Derby, Inkjet printing of functional and structural materials: Fluid property requirements, feature stability, and resolution, Annu. Rev. Mater. Res. (2010). https://doi.org/10.1146/annurev-matsci-070909-104502.

[47] J.A. Inzana, D. Olvera, S.M. Fuller, J.P. Kelly, O.A. Graeve, E.M. Schwarz, S.L. Kates, H.A. Awad, 3D printing of composite calcium phosphate and collagen scaffolds for bone regeneration, Biomaterials. (2014). https://doi.org/10.1016/j.biomaterials.2014.01.064.

[48] T. Boland, X. Tao, B.J. Damon, B. Manley, P. Kesari, S. Jalota, S. Bhaduri, Drop-on-demand printing of cells and materials for designer tissue constructs, Mater. Sci. Eng. C. 27 (2007) 372–376. https://doi.org/10.1016/j.msec.2006.05.047.

[49] W.Y. Yeong, C.K. Chua, K.F. Leong, M. Chandrasekaran, Rapid prototyping in tissue engineering: Challenges and potential, Trends Biotechnol. (2004). https://doi.org/10.1016/j.tibtech.2004.10.004.

[50] M.W. Tibbitt, K.S. Anseth, Hydrogels as extracellular matrix mimics for 3D cell culture, Biotechnol. Bioeng. (2009). https://doi.org/10.1002/bit.22361.

[51] C. Mandrycky, Z. Wang, K. Kim, D.H. Kim, 3D bioprinting for engineering complex tissues, Biotechnol. Adv. (2016). https://doi.org/10.1016/j.biotechadv.2015.12.011.

[52] P.L. Lewis, R.M. Green, R.N. Shah, 3D-printed gelatin scaffolds of differing pore geometry modulate hepatocyte function and gene expression, Acta Biomater. (2018). https://doi.org/10.1016/j.actbio.2017.12.042.

[53] Z. Li, A. Ramos, M.-C. Li, Z. Li, S. Bhatta, A. Jeyaseelan, Y. Li, Q. Wu, S. Yao, J. Xu, Improvement of cell deposition by self-absorbent capability of freeze-dried 3D-bioprinted scaffolds derived from cellulose material-alginate hydrogels, Biomed. Phys. Eng. Express. 6 (2020) 045009. https://doi.org/10.1088/2057-1976/ab8fc6.

[54] S. Anil Kumar, M. Alonzo, S.C. Allen, L. Abelseth, V. Thakur, J. Akimoto, Y. Ito, S.M. Willerth, L. Suggs, M. Chattopadhyay, B. Joddar, A Visible Light-Cross-Linkable, Fibrin-Gelatin-Based Bioprinted Construct with Human Cardiomyocytes and Fibroblasts, ACS Biomater. Sci. Eng. (2019). https://doi.org/10.1021/acsbiomaterials.9b00505.

[55] M.T. Poldervaart, B. Goversen, M. De Ruijter, A. Abbadessa, F.P.W. Melchels, F.C. Öner, W.J.A. Dhert, T. Vermonden, J. Alblas, 3D bioprinting of methacrylated hyaluronic acid (MeHA) hydrogel with intrinsic osteogenicity, PLoS One. (2017). https://doi.org/10.1371/journal.pone.0177628.

[56] Y.B. Kim, H. Lee, G.H. Kim, Strategy to Achieve Highly Porous/Biocompatible Macroscale Cell Blocks, Using a Collagen/Genipin-bioink and an Optimal 3D Printing Process, ACS Appl. Mater. Interfaces. (2016). https://doi.org/10.1021/acsami.6b11669.

[57] S.A. Park, S.J. Lee, J.M. Seok, J.H. Lee, W.D. Kim, I.K. Kwon, Fabrication of 3D Printed PCL/PEG Polyblend Scaffold Using Rapid Prototyping System for Bone Tissue Engineering Application, J. Bionic Eng. 15 (2018) 435–442. https://doi.org/10.1007/s42235-018-0034-8.

[58] T. Billiet, E. Gevaert, T. De Schryver, M. Cornelissen, P. Dubruel, The 3D printing of gelatin methacrylamide cell-laden tissue-engineered constructs with high cell viability, Biomaterials. (2014). https://doi.org/10.1016/j.biomaterials.2013.09.078.

[59] S.E. Bakarich, R. Gorkin, R. Gately, S. Naficy, M. in het Panhuis, G.M. Spinks, 3D printing of tough hydrogel composites with spatially varying materials properties, Addit. Manuf. (2017). https://doi.org/10.1016/j.addma.2016.12.003.

[60] S. Hong, D. Sycks, H.F. Chan, S. Lin, G.P. Lopez, F. Guilak, K.W. Leong, X. Zhao, 3D Printing of Highly Stretchable and Tough Hydrogels into Complex, Cellularized Structures, Adv. Mater. (2015). https://doi.org/10.1002/adma.201501099.

[61] A. Akkineni, T. Ahlfeld, A. Funk, A. Waske, A. Lode, M. Gelinsky, Highly Concentrated Alginate-Gellan Gum Composites for 3D Plotting of Complex Tissue Engineering Scaffolds, Polymers (Basel). (2016). https://doi.org/10.3390/polym8050170.

[62] M. Xu, X. Wang, Y. Yan, R. Yao, Y. Ge, An cell-assembly derived physiological 3D model of the metabolic syndrome, based on adipose-derived stromal cells and a gelatin/alginate/fibrinogen matrix, Biomaterials. (2010). https://doi.org/10.1016/j.biomaterials.2010.01.111.

[63] I.T. Ozbolat, M. Hospodiuk, Current advances and future perspectives in extrusion-based bioprinting, Biomaterials. (2016). https://doi.org/10.1016/j.biomaterials.2015.10.076.

[64] H.J. Lee, Y.B. Kim, S.H. Ahn, J.-S. Lee, C.H. Jang, H. Yoon, W. Chun, G.H. Kim, A New Approach for Fabricating Collagen/ECM-Based Bioinks Using Preosteoblasts and Human Adipose Stem Cells, Adv. Healthc. Mater. 4 (2015) 1359–1368. https://doi.org/10.1002/adhm.201500193.

[65] J.Y. Park, J.C. Choi, J.H. Shim, J.S. Lee, H. Park, S.W. Kim, J. Doh, D.W. Cho, A comparative study on collagen type i and hyaluronic acid dependent cell behavior for osteochondral tissue bioprinting, Biofabrication. (2014). https://doi.org/10.1088/1758-5082/6/3/035004.

[66] N.S. Kajave, T. Schmitt, T.-U. Nguyen, V. Kishore, Dual crosslinking strategy to generate mechanically viable cell-laden printable constructs using methacrylated collagen bioinks, Mater. Sci. Eng. C. 107 (2020) 110290. https://doi.org/10.1016/j.msec.2019.110290.

[67] E. Mirdamadi, J.W. Tashman, D.J. Shiwarski, R.N. Palchesko, A.W. Feinberg, FRESH 3D Bioprinting a Full-Size Model of the Human Heart, ACS Biomater. Sci. Eng. (2020) acsbiomaterials.0c01133. https://doi.org/10.1021/acsbiomaterials.0c01133.

[68] R. Chang, J. Nam, W. Sun, Effects of dispensing pressure and nozzle diameter on cell survival from solid freeform fabrication-based direct cell writing, Tissue Eng. - Part A. (2008). https://doi.org/10.1089/ten.a.2007.0004.

[69] F.J. O'Brien, B.A. Harley, M.A. Waller, I. V. Yannas, L.J. Gibson, P.J. Prendergast, The effect of pore size on permeability and cell attachment in collagen scaffolds for tissue engineering, Technol. Heal. Care. 15 (2006) 3–17. https://doi.org/10.3233/THC-2007-15102.

[70] B. Chevallay, D. Herbage, Collagen-based biomaterials as 3D scaffold for cell cultures: applications for tissue engineering and gene therapy, Med. Biol. Eng. Comput. 38 (2000) 211–218. https://doi.org/10.1007/BF02344779.

[71] C.F. Chang, M.W. Lee, P.Y. Kuo, Y.J. Wang, Y.H. Tu, S.C. Hung, Three-dimensional collagen fiber remodeling by mesenchymal stem cells requires the integrin-matrix interaction, J. Biomed. Mater. Res. - Part A. (2007). https://doi.org/10.1002/jbm.a.30963.

[72] P.N. Christy, S.K. Basha, V.S. Kumari, A.K.H. Bashir, M. Maaza, K. Kaviyarasu, M.V. Arasu, N.A. Al-Dhabi, S. Ignacimuthu, Biopolymeric nanocomposite scaffolds for bone tissue engineering applications – A review, J. Drug Deliv. Sci. Technol. 55 (2020) 101452. https://doi.org/10.1016/j.jddst.2019.101452.

[73] B.R. Seo, X. Chen, L. Ling, Y.H. Song, A.A. Shimpi, S. Choi, J. Gonzalez, J. Sapudom, K. Wang, R.C.A. Eguiluz, D. Gourdon, V.B. Shenoy, C. Fischbach, Collagen microarchitecture mechanically controls myofibroblast differentiation, Proc. Natl. Acad. Sci. U. S. A. (2020). https://doi.org/10.1073/pnas.1919394117.

[74] K.A. Faraj, T.H. van Kuppevelt, W.F. Daamen, Construction of Collagen Scaffolds That Mimic the Three-Dimensional Architecture of Specific Tissues, Tissue Eng. 13 (2007) 2387–2394. https://doi.org/10.1089/ten.2006.0320.

[75] H. Schoof, J. Apel, I. Heschel, G. Rau, Control of pore structure and size in freeze-dried collagen sponges, J. Biomed. Mater. Res. (2001). https://doi.org/10.1002/jbm.1028.

[76] A. Rouhollahi, O. Ilegbusi, S. Florczyk, K. Xu, H. Foroosh, Effect of Mold Geometry on Pore Size in Freeze-Cast Chitosan-Alginate Scaffolds for Tissue Engineering, Ann. Biomed. Eng. 48 (2020) 1090–1102. https://doi.org/10.1007/s10439-019-02381-3.

[77] T. Guo, T.R. Holzberg, C.G. Lim, F. Gao, A. Gargava, J.E. Trachtenberg, A.G. Mikos, J.P. Fisher, 3D printing PLGA: A quantitative examination of the effects of polymer composition and printing parameters on print resolution, Biofabrication. (2017). https://doi.org/10.1088/1758-5090/aa6370.

[78] L.A. Hockaday, K.H. Kang, N.W. Colangelo, P.Y.C. Cheung, B. Duan, E. Malone, J. Wu, L.N. Girardi, L.J. Bonassar, H. Lipson, C.C. Chu, J.T. Butcher, Rapid 3D printing of anatomically accurate and mechanically heterogeneous aortic valve hydrogel scaffolds, Biofabrication. 4 (2012) 035005. https://doi.org/10.1088/1758-5082/4/3/035005.

[79] R. Schipani, D.R. Nolan, C. Lally, D.J. Kelly, Integrating finite element modelling and 3D printing to engineer biomimetic polymeric scaffolds for tissue engineering, Connect. Tissue Res. (2020). https://doi.org/10.1080/03008207.2019.1656720.

[80] M.M. Laronda, A.L. Rutz, S. Xiao, K.A. Whelan, F.E. Duncan, E.W. Roth, T.K. Woodruff, R.N. Shah, A bioprosthetic ovary created using 3D printed microporous scaffolds restores ovarian function in sterilized mice, Nat. Commun. (2017). https://doi.org/10.1038/ncomms15261.

[81] P. Diloksumpan, M. ne De Ruijter, M. Castilho, U. Gbureck, T. Vermonden, P.R. Van Weeren, J. Malda, R. Levato, Combining multi-scale 3D printing technologies to engineer reinforced hydrogel-ceramic interfaces, Biofabrication. (2020). https://doi.org/10.1088/1758-5090/ab69d9.

[82] T. Mohan, A. Dobaj Štiglic, M. Beaumont, J. Konnerth, F. Gürer, D. Makuc, U. Maver, L. Gradišnik, J. Plavec, R. Kargl, K. Stana Kleinschek, Generic Method for Designing Self-Standing and Dual Porous 3D Bioscaffolds from Cellulosic Nanomaterials for Tissue Engineering Applications, ACS Appl. Bio Mater. 3 (2020) 1197–1209. https://doi.org/10.1021/acsabm.9b01099.

[83] G. Filardo, M. Petretta, C. Cavallo, L. Roseti, S. Durante, U. Albisinni, B. Grigolo, Patient-specific meniscus prototype based on 3D bioprinting of human cell-laden scaffold, Bone Joint Res. 8 (2019) 101–106. https://doi.org/10.1302/2046-3758.82.BJR-2018-0134.R1.

[84] H.N. Chia, B.M. Wu, Recent advances in 3D printing of biomaterials, J. Biol. Eng. (2015). https://doi.org/10.1186/s13036-015-0001-4.

[85] K. Anselme, L. Ploux, A. Ponche, Cell/Material Interfaces: Influence of Surface Chemistry and Surface Topography on Cell Adhesion, J. Adhes. Sci. Technol. 24 (2010) 831–852. https://doi.org/10.1163/016942409X12598231568186.

[86] J. Zhang, A. Zhou, A. Deng, Y. Yang, L. Gao, Z. Zhong, S. Yang, Pore architecture and cell viability on freeze dried 3D recombinant human collagen-peptide (RHC)–chitosan scaffolds, Mater. Sci. Eng. C. 49 (2015) 174–182. https://doi.org/10.1016/j.msec.2014.12.076.

[87] C.A. Schneider, W.S. Rasband, K.W. Eliceiri, NIH Image to ImageJ: 25 years of image analysis, Nat. Methods. 9 (2012) 671–675. https://doi.org/10.1038/nmeth.2089.

[88] J. Ma, Im2mesh (2D image to triangular meshes), MATLAB Cent. File Exch. (2020). https://www.mathworks.com/matlabcentral/fileexchange/71772-im2mesh-2d-image-to-triangular-meshes (accessed September 25, 2020).

[89] K.L. Scotti, D.C. Dunand, Freeze casting – A review of processing, microstructure and properties via the open data repository, FreezeCasting.net, Prog. Mater. Sci. 94 (2018) 243–305. https://doi.org/10.1016/j.pmatsci.2018.01.001.

[90] S. Wang, Y. Yang, G.L. Koons, A.G. Mikos, Z. Qiu, T. Song, F. Cui, X. Wang, Tuning pore features of mineralized collagen/PCL scaffolds for cranial bone regeneration in a rat model, Mater. Sci. Eng. C. 106 (2020) 110186. https://doi.org/10.1016/j.msec.2019.110186.

[91] Y.-C. Lin, F. Tan, K.G. Marra, S.-S. Jan, D.-C. Liu, Synthesis and characterization of collagen/hyaluronan/chitosan composite sponges for potential biomedical applications, Acta Biomater. 5 (2009) 2591–2600. https://doi.org/10.1016/j.actbio.2009.03.038.

[92] B.A. Harley, J.H. Leung, E.C.C.M. Silva, L.J. Gibson, Mechanical characterization of collagen-glycosaminoglycan scaffolds, Acta Biomater. (2007). https://doi.org/10.1016/j.actbio.2006.12.009.

[93] S. Lin, M.C. Lampi, C.A. Reinhart-King, G. Tsui, J. Wang, C.A. Nelson, L. Gu, Eigenstrain as a mechanical set-point of cells, Biomech. Model. Mechanobiol. (2018). https://doi.org/10.1007/s10237-018-1004-0.

[94] Q. Zhang, H. Lu, N. Kawazoe, G. Chen, Pore size effect of collagen scaffolds on cartilage regeneration, Acta Biomater. (2014). https://doi.org/10.1016/j.actbio.2013.12.042.

[95] C.M. Murphy, A. Matsiko, M.G. Haugh, J.P. Gleeson, F.J. O'Brien, Mesenchymal stem cell fate is regulated by the composition and mechanical properties of collagen–glycosaminoglycan scaffolds, J. Mech. Behav. Biomed. Mater. 11 (2012) 53–62. https://doi.org/10.1016/j.jmbbm.2011.11.009.

[96] E. Cenni, F. Perut, N. Baldini, In vitro models for the evaluation of angiogenic potential in bone engineering, Acta Pharmacol. Sin. 32 (2011) 21–30. https://doi.org/10.1038/aps.2010.143.

[97] R.E. Unger, A. Sartoris, K. Peters, A. Motta, C. Migliaresi, M. Kunkel, U. Bulnheim, J. Rychly, C. James Kirkpatrick, Tissue-like self-assembly in cocultures of endothelial cells and osteoblasts and the formation of microcapillary-like structures on three-dimensional porous biomaterials, Biomaterials. (2007). https://doi.org/10.1016/j.biomaterials.2007.05.032.